3-2006

Investigation of Frequency-Domain and Time-Domain Free-Space Material Measurements

Kirt J. Cassell

Investigation of Frequency-Domain and Time-Domain Free-Space Material Measurements

THESIS

Kirt J. Cassell, Captain, USAF

AFIT/GE/ENG/06-12

DEPARTMENT OF THE AIR FORCE
AIR UNIVERSITY

AIR FORCE INSTITUTE OF TECHNOLOGY

Wright-Patterson Air Force Base, Ohio

AFIT/GE/ENG/06-12

Investigation of Frequency-Domain and Time-Domain Free-Space Material Measurements

THESIS

Presented to the Faculty

Department of Electrical and Computer Engineering

Graduate School of Engineering and Management

Air Force Institute of Technology

Air University

Air Education and Training Command

In Partial Fulfillment of the Requirements for the

Degree of Master of Science in Electrical Engineering

Kirt J. Cassell, B.S.E.E., MBA

Captain, USAF

March 2006

AFIT/GE/ENG/06-12

Investigation of Frequency-Domain and Time-Domain Free-Space Material Measurements

Kirt J. Cassell, B.S.E.E., MBA
Captain, USAF

Approved:

/signed/	23 Mar 2006
Dr. Michael J. Havrilla (Chairman)	date
/signed/	23 Mar 2006
Dr. Andrew J. Terzuoli (Member)	date
/signed/	23 Mar 2006
Dr. William P. Baker (Member)	date

Abstract

Electromagnetic material characterization is the process of determining the complex permittivity and permeability of a test sample. The primary goal of this thesis is to develop a new two transmission material measurement method to decrease the error associated with using a reflection measurement. The transmission method uses a sample transmission measurement and a acrylic backed sample transmission measurement. This technique is first demonstrated in a rectangular waveguide system then extended to frequency-domain and time-domain focus arch free-space systems.

Most free-space systems consist of transmit and receive spot-focusing horn lens antennas and a network analyzer (NWA). A six step procedure is used to extract the material characteristics using the NWA. The data is measured (1) using the NWA then it is frequency windowed (2) to knock down the sidelobes that appear in the time-domain after the data is transformed. Once transformed (3) to the time-domain the data is time gated (4) to eliminate multiple reflections between the antennas and sample. The data is transformed (5) back into the frequency-domain for extraction (6) of permittivity and permeability using a Nicolson-Ross-Weir (NRW) method and two transmission method. Windowing and transforming the data, steps two and three, decreases accuracy at the band edges. The use of a digital oscilloscope with a time-domain reflectometer (TDR) module should increase accuracy by removing the windowing and transforming operations. Thus, a secondary goal of this thesis is to analyze the effect on material characterization accuracy using an oscilloscope instead of a NWA since one window and one transform operation is removed.

Experimental results of the permittivity and permeability values of a magnetic radar absorbing material (MRAM) sample for the three measuring devices are presented. The two transmission method is compared to the NRW method in the waveguide and frequency-domain focus arch system to validate the two transmission

method. A differential uncertainty analysis is conducted to show the improved accuracy of the two transmission method over a reflection measurement based parameter extraction technique such as the NRW method. A comparison of the time-domain and frequency-domain focused arch results is also conducted.

Acknowledgements

First and foremost, I would like to thank Dr. Havrilla for his leadership and knowledge that ensured my completion of this thesis. I would also like to thank my committee Dr. Terzuoli and Dr. Baker for their contribution to my thesis. Mr. Glen Hilderbrand and Mr. John Nelson at GE in Cincinnati are the backbone of my work without them I would have no data. Thanks to Dr. Peter Munk and Mr. Rodney George at AFRL/SNS for there support. I owe all of my success in this thesis and the AFIT program to my loving family. To my lovely daughter thank you for the smiles and hugs when daddy came home from a hard day at work. To my new son thank you for sleeping through the night. To my wife the love of my life without whom none of my endeavors would be successful. Thank you.

Kirt J. Cassell

Table of Contents

Page

List of Figures

List of Abbreviations

Investigation of Frequency-Domain and Time-Domain Free-Space Material Measurements

I. Introduction

Material characterization is the process of determining the relative constitutive parameters permittivity and permeability (ϵ_r,μ_r) of a material. The permittivity of a material determines its susceptibility to being electrically polarized when in the presence of an electric field. Likewise, the permeability of a material determines its susceptibility to being magnetically polarized when in the presence of an magnetic field. Generally, permittivity and permeability are complex quantities, where the real parts are related to energy storage and the imaginary parts are related to energy loss.

Radar absorbing materials have many uses such as clutter suppression at airports, electromagnetic shielding used in electromagnetic compatibility (EMC) applications, as well as in compact ranges and anechoic chambers. The Air Force uses radar absorbing material (RAM) on many of its low observable aircraft. The increasing application of RAM requires greater need for accurate constitutive parameter measurements.

This thesis presents a new transmission only material measurement technique and differential uncertainty analysis. The technique is used to extract ϵ_r and μ_r of a sample and is first demonstrated in a waveguide system. Then extended to a frequency-domain and time-domain free-space focus arch system aimed at increasing measurement accuracy and decreasing processing time and resources.

1.1 Problem Statement

In general most material parameters are extracted using a reflection and transmission measurement. The use of a reflection measurement can introduce large error

due to the position dependence of the reflection measurement. One method to overcome this error is the use of two transmission measurements of the same material with different thicknesses. However, an argument can be made that although these two pieces of material with differing thicknesses come from the same stock they are indeed different due to sample fabrication and mixing inconsistencies. This thesis offers a material measurement technique that uses one thickness of material and backs it by a known sample thus allowing for accurate measurements of a single piece of material using only transmission measurements.

A material characterization process for a waveguide system consists of several basic steps. A Thru-Reflect-Line (TRL) calibration is used to calibrate the waveguide system. The sample must be accurately machined to fill the waveguide holder to ensure that only the dominate waveguide mode is present. A NWA is used to measure the reflected and transmitted scattering parameters (S-parameters) of the material. Numerical algorithms such as the NRW method [1, 6, 8, 10, 11] are then used to extract the complex permittivity and permeability from these S-parameters. The NRW technique requires a transmission and reflection measurement and will be used to show the error caused by using a reflection measurement. If the NRW algorithm cannot be used an iterative method such as a Newton Two-Dimensional (2D) root search is applied. The use of a reflection measurement can lead to large error due to the path length difference that can occur when making a reflection measurement as shown in Figure 1.1. A position correction factor and the use of both forward and reverse measurements can be used to account for this error. It will be shown that the use of transmission measurements which are independent of sample position eliminates the need for a correction factor and leads to more accurate results.

The material characterization process for a focus arch free-space system is somewhat different from the waveguide system. The focus arch system consists of two wide band antennas, two dielectric lenses, a sample holder, and a NWA. The sample is placed in the holder between two dielectric focusing lenses which are themselves between two wide band antennas. The NWA is then connected to the antennas and

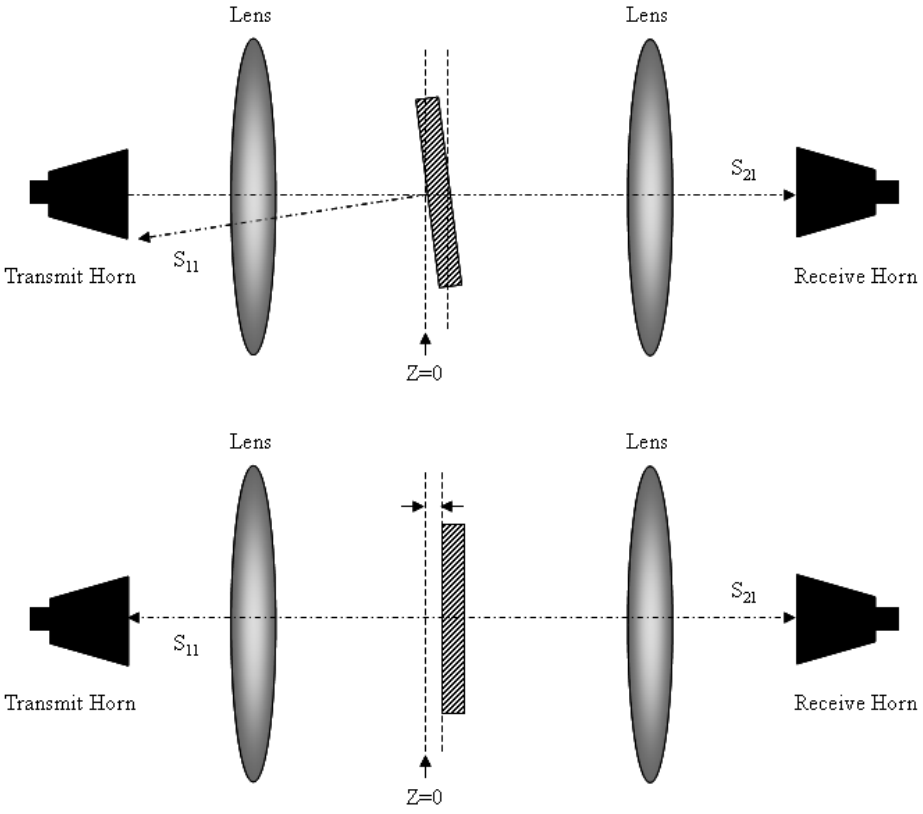

Figure 1.1: Focus arch system depicting the two types of reflection measurement error that can occur. One error source is caused by the sample not being normal to the incident wave causing a increase in path length. The second error source is caused by the sample not being located at the $Z = 0$ reference plane.

the S-parameters of the material are measured. The lenses serve to collimate (equal phase front) and focus the beam on the material. As with the waveguide system the NRW method and two transmission method are used to extract the ϵ_r and μ_r from the measured S-parameters. Prior to applying an extraction algorithm a calibration process must be conducted. The experimental data is frequency windowed to knock down the sidelobes that occur when transformed to the time-domain. This frequency windowing step causes a loss of accurate data at the band edges. Once in the time-domain the data is time gated to remove unwanted sample antenna interactions. Finally, the data is transformed back into the frequency-domain and a numerical algorithm is applied.

The material characterization process for a focus arch free-space system can be further simplified by using a time-domain system. Replacing the NWA with a digital oscilloscope having a Time-Domain Transmission (TDT) module allows for direct time-domain measurement of the sample. Eliminating the need to frequency window and transform to the time-domain improving band edge data. The direct time-domain measurements are then gated as above and transformed to the frequency-domain for parameter extraction.

The goal of this thesis is to first demonstrate the two transmission technique in a rectangular waveguide system eliminating error associated with the reflection measurement. The transmission method is then extended to a free-space frequency-domain focus arch system. Lastly, the technique is further extended to direct time-domain free-space measurements which will increase band edge accuracy and reduce data processing time.

1.2 Scope

Many other measurement devices can be used for material characterization including, but not limited to, circular waveguide systems, stripline systems, and coaxial waveguide systems. This thesis will explore S-band (2.6-3.95 Gigahertz (GHz)) and

X-band (8.2-12.4 GHz) rectangular waveguide applications as well as both frequency-domain and time-domain focus arch free-space (2-18 GHz) applications.

1.3 Organization

Chapter 2 provides a review of S-parameters and wave transmission matrices (A-parameters) along with the NRW algorithm for a waveguide and free-space system. Chapter 3 presents a two transmission method for extracting constitutive parameters for a waveguide system and free-space system. Chapter 4 presents results for S-band and X-band waveguide transmission measurements and an analysis of frequency-domain and time-domain free-space results is also included. Finally, conclusions and recommendations for future research are given in Chapter 5.

II. Background

This chapter provides the necessary background for understanding the measurement methods used in this thesis.

2.1 A-Parameter Single Layer System

A-parameters are a simple method to solve single and multi-layered systems. The development describes the relationship between incident and reflected wave amplitudes at the input and output terminal plane. The A-parameter description of a single layer system is examined first then generalized to a N-layer system in the following section. An expanded view of a single-layered environment is shown in Figure 2.1. If R_1, T_{12} and R_2, T_{21} are the respective interfacial reflection and transmission coefficients due to waves c_1 and b_2' then the following relations exist.

$$\begin{aligned} c_2^{'} &= T_{12}c_1 + R_2 b_2^{'} \\ b_1 &= R_1 c_1 + T_{21} b_2^{'} \end{aligned} \tag{2.1}$$

where the reflection and transmission equations are

$$\begin{aligned} T_1 &= T_{12} = 1 + R_1 \\ T_2 &= T_{21} = 1 + R_2 \\ R_1 &= -R_2 = \frac{Z_2 - Z_1}{Z_2 + Z_1} \end{aligned} \tag{2.2}$$

Substituting (2.2) into (2.1) leads to the matrix expression

$$\begin{bmatrix} c_1 \\ b_1 \end{bmatrix} = \frac{1}{T_1} \begin{bmatrix} 1 & R_1 \\ R_1 & 1 \end{bmatrix} \begin{bmatrix} c_2^{'} \\ b_2^{'} \end{bmatrix} \tag{2.3}$$

Equation (2.3) describes the relationship between the incident and reflected traveling waves (c_1, b_1) and $(c_2^{'}, b_2^{'})$ immediately to the left and right of the sample interface, respectively. It is necessary to show how the waves $(c_2^{'}, b_2^{'})$ are related to waves (c_2, b_2)

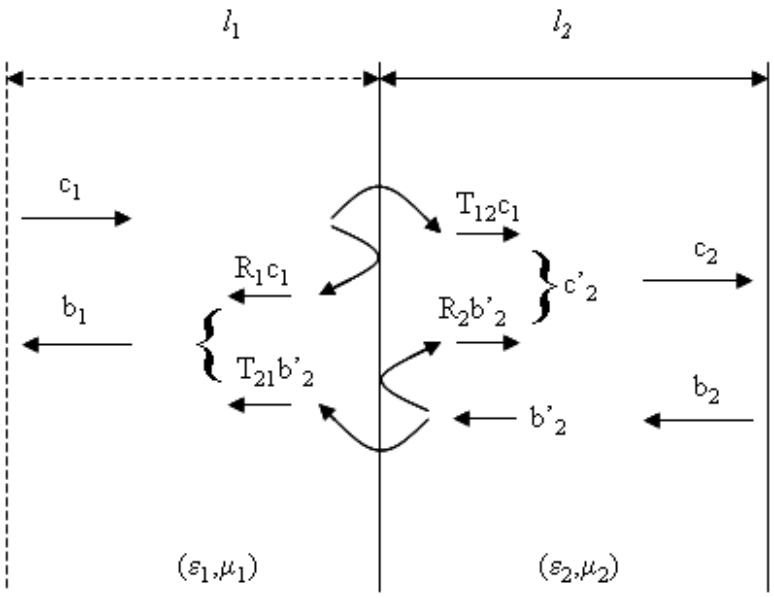

Figure 2.1: Single layer system showing the relationship between the reflected and transmitted coefficients and the interfacial reflection and transmission coefficients.

located a distance l_2 from the interface as shown in Figure (2.1). The sample region is assumed to be linear, homogeneous, and isotropic (simple media) therefore, the following relation exists between the waves.

$$\begin{aligned} c_2^{'} &= c_2 e^{\gamma_2 l_2} \\ b_2^{'} &= b_2 e^{-\gamma_2 l_2} \end{aligned} \tag{2.4}$$

This relationship can be written in matrix form

$$\begin{bmatrix} c_2^{'} \\ b_2^{'} \end{bmatrix} = \begin{bmatrix} e^{\gamma_2 l_2} & 0 \\ 0 & e^{-\gamma_2 l_2} \end{bmatrix} \begin{bmatrix} c_2 \\ b_2 \end{bmatrix} \tag{2.5}$$

The A-parameter relationship between waves (c_1, b_1) and (c_2, b_2) is obtained by substituting (2.5) into (2.3).

$$\begin{bmatrix} c_1 \\ b_1 \end{bmatrix} = \frac{1}{T_1} \begin{bmatrix} e^{\gamma_2 l_2} & R_1 e^{-\gamma_2 l_2} \\ R_1 e^{\gamma_2 l_2} & e^{-\gamma_2 l_2} \end{bmatrix} \begin{bmatrix} c_2 \\ b_2 \end{bmatrix} = \begin{bmatrix} A_{11} & A_{12} \\ A_{21} & A_{22} \end{bmatrix} \begin{bmatrix} c_2 \\ b_2 \end{bmatrix} \tag{2.6}$$

The relationship between A-parameters and S-parameters is found using the below equation

$$b_1 = S_{11} c_1 + S_{12} b_2 \tag{2.7}$$

$$c_2 = S_{21} c_1 + S_{22} b_2 \tag{2.8}$$

Solving (2.8) for the incident wave, c_1 gives the following

$$c_1 = \frac{1}{S_{21}} c_2 - \frac{S_{22}}{S_{21}} b_2 \tag{2.9}$$

where the coefficients of c_2 and b_2 are A_{11} and A_{12}, respectively. Substituting (2.9) into (2.7) gives the equation for the reflected wave shown below

$$b_1 = S_{11} \left(\frac{1}{S_{21}} c_2 - \frac{S_{22}}{S_{21}} b_2 \right) + S_{12} b_2 \tag{2.10}$$

Rearranging and grouping terms leads to the below equation for the reflected wave

$$b_1 = \frac{S_{11}}{S_{21}} c_2 + \left(\frac{S_{11} S_{22} - S_{12} S_{21}}{S_{21}} \right) b_2 \tag{2.11}$$

where the coefficients of c_2 and b_2 are A_{21} and A_{22}, respectively. The relationship between S-parameters and A-parameters are shown below in matrix form.

$$\begin{bmatrix} A_{11} & A_{12} \\ A_{21} & A_{22} \end{bmatrix} = \frac{1}{S_{21}} \begin{bmatrix} 1 & -S_{22} \\ S_{11} & S_{21} S_{12} - S_{11} S_{22} \end{bmatrix} \tag{2.12}$$

$$\begin{bmatrix} S_{11} & S_{12} \\ S_{21} & S_{22} \end{bmatrix} = \frac{1}{A_{11}} \begin{bmatrix} A_{21} & A_{11}A_{22} - A_{21}A_{12} \\ 1 & -A_{12} \end{bmatrix} \tag{2.13}$$

Applying the above relationship to (2.6) leads to the theoretical forward S-parameters of a single-layered material

$$S_{11}^{thy} = \frac{R(1-P^2)}{1-R^2P^2} \tag{2.14}$$

$$S_{21}^{thy} = \frac{P(1-R^2)}{1-R^2P^2} \tag{2.15}$$

where R is the reflection coefficient and P is the one-way phase delay through the material given by [6], [3].

$$\begin{aligned} P &= e^{-\gamma\ell} \\ R &= \frac{Z_2 - Z_1}{Z_2 + Z_1} \end{aligned} \tag{2.16}$$

2.2 A-Parameter Multi-Layered System

Figure 2.2 shows a multi-layered system in free-space, comprised of $N-1$ layers and N interfaces. The c_i, b_i terms are the incident and reflected complex wave amplitudes to the left of the i^{th} interface. The length, complex permittivity, and complex permeability of the i^{th} layer are denoted by l_i, ϵ_i, and μ_i, respectively. The interfacial reflection and transmission coefficients of the i^{th} interface are denoted by R_i and T_i. From the single layer analysis above an overall A-parameter description of a cascaded N-layer system can be obtained by generalizing (2.6)

$$\begin{bmatrix} c_1 \\ b_1 \end{bmatrix} = \prod_{i=1}^{N+1} \frac{1}{T_i} \begin{bmatrix} e^{\gamma_i l_i} & R_i e^{-\gamma_i l_i} \\ R_i e^{\gamma_i l_i} & e^{-\gamma_i l_i} \end{bmatrix} \begin{bmatrix} c_{N+1} \\ b_{N+1} \end{bmatrix} = \begin{bmatrix} A_{11}^{sys} & A_{12}^{sys} \\ A_{21}^{sys} & A_{22}^{sys} \end{bmatrix} \begin{bmatrix} c_{N+1} \\ b_{N+1} \end{bmatrix} \tag{2.17}$$

solving for the system A-parameters leads to the following result

$$\begin{bmatrix} A_{11}^{sys} & A_{12}^{sys} \\ A_{21}^{sys} & A_{22}^{sys} \end{bmatrix} = \prod_{i=1}^{N+1} \frac{1}{T_i} \begin{bmatrix} e^{\gamma_i l_i} & R_i e^{-\gamma_i l_i} \\ R_i e^{\gamma_i l_i} & e^{-\gamma_i l_i} \end{bmatrix} = \prod_{i=1}^{N+1} \begin{bmatrix} A_{11}^{i} & A_{12}^{i} \\ A_{21}^{i} & A_{22}^{i} \end{bmatrix} \tag{2.18}$$

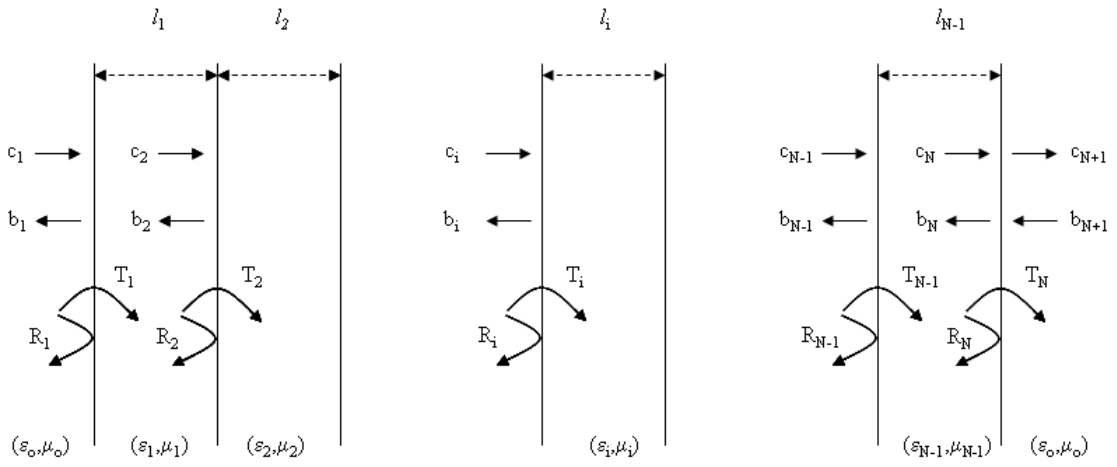

Figure 2.2: A multi-layered system in free-space, comprised of $N-1$ layers and N interfaces. The system shows the relationship between the reflected and transmitted coefficients and the interfacial reflection and transmission coefficients.

where

$$\begin{aligned} R_i &= \frac{Z_i - Z_{i-1}}{Z_i + Z_{i-1}} \\ T_i &= 1 + R_i \\ P_i &= e^{-\gamma_i l_i} \end{aligned} \tag{2.19}$$

As an example consider the two-layered sample of length l_{sys} immersed in free-space shown in Figure 2.3. There are three interfaces that result in the following specialization of (2.17)

$$\begin{bmatrix} c_1 \\ b_1 \end{bmatrix} = \prod_{i=1}^{3} \frac{1}{T_i} \begin{bmatrix} e^{\gamma_i l_i} & R_i e^{-\gamma_i l_i} \\ R_i e^{\gamma_i l_i} & e^{-\gamma_i l_i} \end{bmatrix} \begin{bmatrix} c_4 \\ b_4 \end{bmatrix} = \begin{bmatrix} A_{11}^{sys} & A_{12}^{sys} \\ A_{21}^{sys} & A_{22}^{sys} \end{bmatrix} \begin{bmatrix} c_4 \\ b_4 \end{bmatrix} \tag{2.20}$$

$l_3 = 0$ and letting $P_i = e^{-\gamma_i l_i}$ the wave matrix for the system is therefore,

$$\begin{bmatrix} A_{ii}^{sys} \end{bmatrix} = \frac{1}{T_1 T_2 T_3} \begin{bmatrix} P_1^{-1} & R_1 P_1 \\ R_1 P_1^{-1} & P_1 \end{bmatrix} \begin{bmatrix} P_2^{-1} & R_2 P_2 \\ R_2 P_2^{-1} & P_2 \end{bmatrix} \begin{bmatrix} 1 & R_3 \\ R_3 & 1 \end{bmatrix} \tag{2.21}$$

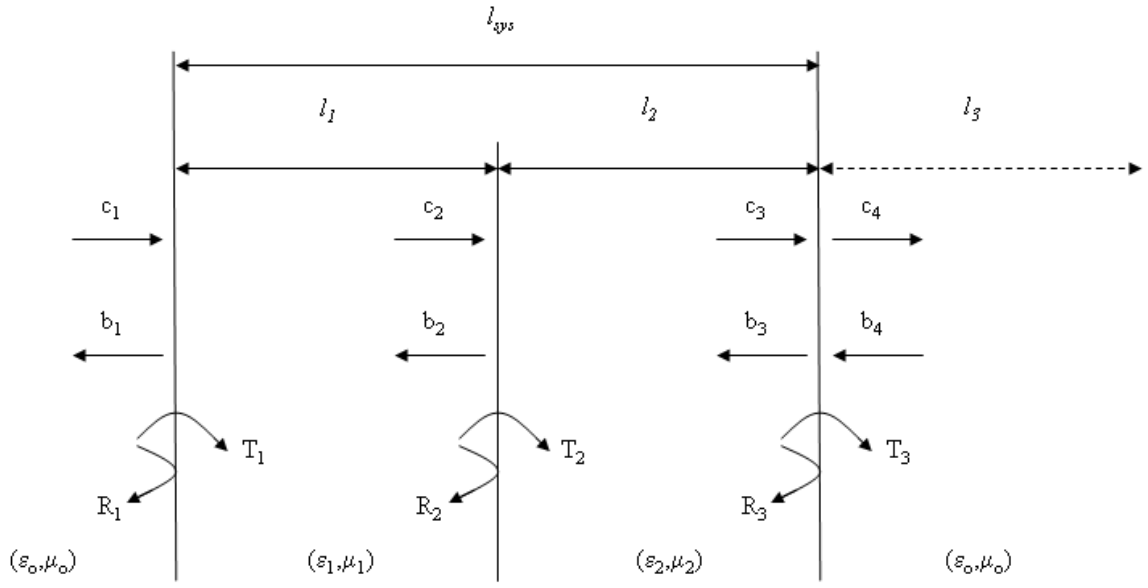

Figure 2.3: Two-layered sample of length l_{sys} immersed in free-space showing the relationship between the reflected and transmitted coefficients and the interfacial reflection and transmission coefficients.

where $Z_o = \sqrt{\frac{\mu_o}{\epsilon_o}}$ representing the air layer [6].

$$\begin{aligned} R_1 &= \frac{Z_1 - Z_o}{Z_1 + Z_o} \\ T_1 &= 1 + R_1 \\ R_2 &= \frac{Z_2 - Z_1}{Z_2 + Z_1} \\ T_2 &= 1 + R_2 \\ R_3 &= \frac{Z_o - Z_2}{Z_o + Z_2} \\ T_3 &= 1 + R_3 \\ P_i &= e^{-\gamma_i l_i} \end{aligned} \tag{2.22}$$

2.3 NRW Algorithm

Material measurements compare the theoretical S-parameters (S_{11}^{thy},S_{21}^{thy}) to experimentally measured sample S-parameters (S_{11}^{exp},S_{21}^{exp})

$$\begin{aligned} S_{21}^{thy,M1}(\omega,\epsilon,\mu) - S_{21}^{exp,M1}(\omega) &= 0 \\ S_{21}^{thy,M2}(\omega,\epsilon,\mu) - S_{21}^{exp,M2}(\omega) &= 0 \end{aligned} \tag{2.23}$$

Nicolson, Ross, and Weir combined (2.9) and (2.10) and derived explicit formulas for a material's constitutive parameters ϵ_r and μ_r. Similarly to the theoretical S-parameter values the experimental S-parameters can be written as

$$S_{11}^{exp} = \frac{R(1-P^2)}{1-R^2P^2} \tag{2.24}$$

$$S_{21}^{exp} = \frac{P(1-R^2)}{1-R^2P^2} \tag{2.25}$$

The NRW formulas are derived by first solving (2.24) for P^2 and (2.25) for P

$$P^2 = \frac{R - S_{11}^{exp}}{R(1-RS_{11}^{exp})} \tag{2.26}$$

$$P = \frac{S_{21}^{exp}(1-R^2P^2)}{1-R^2} \tag{2.27}$$

Substituting (2.26) into the P^2 term of (2.27) leads to

$$P = \frac{S_{21}^{exp}}{1-RS_{11}^{exp}} \Rightarrow P^2 = \left(\frac{S_{21}^{exp}}{1-RS_{11}^{exp}}\right)^2 \tag{2.28}$$

After equating (2.26) and (2.28)

$$\frac{R - S_{21}^{exp}}{R(1-RS_{11}^{exp})} = \left(\frac{S_{21}^{exp}}{1-RS_{11}^{exp}}\right)^2 \Rightarrow \frac{R - S_{11}^{exp}}{R} = \frac{(S_{21}^{exp})^2}{1-RS_{11}^{exp}} \tag{2.29}$$

Simplifying and grouping terms leads to the following quadratic equation

$$R^2 - 2KR + 1 \tag{2.30}$$

where

$$K = \frac{(S_{11}^{exp})^2 - (S_{21}^{exp})^2 + 1}{2S_{11}^{exp}} \tag{2.31}$$

whose solution is

$$R = K \pm \sqrt{K^2 - 1} \tag{2.32}$$

The correct choice of positive or negative sign in (2.32) is made by requiring $|R| < 1$. The thickness of the material is chosen such that S_{11}^{exp} in (2.31) does not equal zero. The phase delay through the material P is given by the following

$$P = \frac{S_{21}^{\text{exp}}}{1 - RS_{11}^{\text{exp}}} \tag{2.33}$$

The below equations are used to find the constitutive parameters (ϵ_r,μ_r) of a sample of length l in a rectangular waveguide operating in the fundamental transverse electric (TE) mode

$$\mu_r = \frac{-\ln P}{\gamma_0 \ell}\left(\frac{1+R}{1-R}\right) \tag{2.34}$$

$$\varepsilon_r = \frac{k_c^2 - \gamma^2}{\mu_r k_0^2} \tag{2.35}$$

where

$$\begin{aligned} k_c^2 &= \frac{\pi^2}{a^2} \\ k_0^2 &= \omega^2 \varepsilon_0 \mu_0 \\ \gamma_0^2 &= k_c^2 - k_0^2 \end{aligned} \tag{2.36}$$

The constitutive parameters for a transverse electromagnetic (TEM) system can be easily found by letting $k_c = 0$ reducing the above waveguide method to a TEM method [6], [2].

2.4 Discrete Fourier Transform

There is a large amount of data processing for the calibration of the free-space system including transformations to and from the frequency-domain and time-domain. Therefore, the discrete fourier transform is outlined below and interested readers can obtain a further review of Discrete Fourier Transforms (DFT) in, 'Signal Processing and Linear Systems,' by B. P. Lathi [9].

The following equations define the discrete DFT with F_n the direct DFT of f_k, and f_k the inverse discrete Fourier transform (IDFT) of F_n.

$$\begin{aligned} F_n &= \sum_{k=0}^{N_0-1} f_k e^{-jn\frac{2\pi}{N_0}k} \\ f_k &= \frac{1}{N_0}\sum_{n=0}^{N_0-1} F_n e^{jn\frac{2\pi}{N_0}k} \end{aligned} \tag{2.37}$$

The notation $f_k \Leftrightarrow F_n$ denotes a DFT pair. F_n is the n^{th} sample of $F(\omega)$ and f_k is T_0/N_0 times the k^{th} sample of $f(t)$. If the sample values of $f(t)$ are known then the sample values of $F(\omega)$ can be computed and vice versa using the DFT. f_k is a function of k $(k = 0, 1, 2, ...N_0 - 1)$ rather than that of t and F_n is a function of n $(n = 0, 1, 2, ...N_0 - 1)$ rather than ω. A sampled signal $\bar{f}(t)$ can be expressed as

$$\bar{f}(t) = \sum_{k=0}^{N_0-1} f(kT)\delta(t - kT) \tag{2.38}$$

$$\delta(t - kT) \Leftrightarrow e^{-jk\omega t} \tag{2.39}$$

$$\omega = \frac{2\pi}{T} \tag{2.40}$$

The Fourier transform of (2.38) yields

$$\bar{F}(\omega) = \sum_{k=0}^{N_0-1} f(kT)e^{-jk\omega t} \tag{2.41}$$

However, over the interval $|\omega| \leq \frac{\omega_s}{2}$, $\bar{F}(\omega)$ of $\bar{f}(t)$ is $\frac{F(\omega)}{T}$, assuming negligible aliasing

$$F(\omega) = T\bar{F}(\omega) = T\sum_{k=0}^{N_0-1} f(kT)e^{-jk\omega T} \tag{2.42}$$

and

$$F_n = F(n\omega_0) = T\sum_{k=0}^{N_0-1} f(kT)e^{-jkn\omega_0 T} \tag{2.43}$$

Observing the fact that N_0, the number of samples of a signal in one period T_0 is identical to N_0'.

$$N_0 = \frac{T_0}{T} \tag{2.44}$$

$$F_0 = \frac{1}{T_0} \tag{2.45}$$

$$N_0 = \frac{T_0}{T} = N_0' \tag{2.46}$$

Also, substituting $Tf(kT) = f_k$ yields the equation for the DFT

$$F_n = \sum_{k=0}^{N_0-1} f_k e^{-jn\frac{2\pi}{N_0}k} \tag{2.47}$$

To find the inverse relation multiply both sides of (2.47) by $e^{jm\frac{2\pi}{N_0}n}$

$$\sum_{n=0}^{N_0-1} F_n e^{jm\frac{2\pi}{N_0}n} = \sum_{n=0}^{N_0-1}\left[\sum_{k=0}^{N_0-1} f_k e^{-jn\frac{2\pi}{N_0}k}\right] e^{jm\frac{2\pi}{N_0}n} \tag{2.48}$$

Interchanging the summation on the right hand side

$$\sum_{n=0}^{N_0-1} F_n e^{jm\frac{2\pi}{N_0}n} = \sum_{k=0}^{N_0-1} f_k \left[\sum_{n=0}^{N_0-1} e^{j(m-k)\frac{2\pi}{N_0}n} \right] \tag{2.49}$$

The inner sum on the right hand side is zero for $k \neq m$, and N_0 when $k = m$ shown below

$$\sum_{n=0}^{N_0-1} e^{j(m-k)\frac{2\pi}{N_0}n} = N_0 \delta_{m,k} \tag{2.50}$$

Therefore, $N_0 f_k = N_0 f_m$ which yields the equation for the IDFT

$$f_m = \frac{1}{N_0} \sum_{n=0}^{N_0-1} F_n e^{jm\frac{2\pi}{N_0}n} \tag{2.51}$$

III. Methodology

This chapter presents a transmission only method to extract the constitutive parameters of a test sample mounted in a rectangular waveguide and a free-space system. The analysis will result in a calculated S-parameter for both the single-layer sample, $S_{21}^{thy,M1}$ and the two-layer acrylic backed sample, $S_{21}^{thy,M2}$. The theoretical values will be compared to corresponding single-layer sample measurements, $S_{21}^{exp,M1}$, and two-layer acrylic backed sample measurements, $S_{21}^{exp,M2}$. Using an iterative Newton 2D root search the sample's material parameters will be those theoretical values of ϵ_r,μ_r that satisfy the below equations to within a specified accuracy at each frequency:

$$\begin{aligned} |S_{21}^{thy,M1}(\omega,\epsilon_r,\mu_r) - S_{21}^{exp,M1}(\omega)| &< accuracy \\ |S_{21}^{thy,M2}(\omega,\epsilon_r,\mu_r) - S_{21}^{exp,M2}(\omega)| &< accuracy \end{aligned} \tag{3.1}$$

The results of the two transmission method will be compared to the NRW method. It will be shown that the two transmission method removes path length dependent reflection errors associated with the NRW method.

3.1 Acrylic Sample

To solve for both ϵ_r and μ_r it is necessary to have two independent transmission measurements. The first measurement, $S_{21}^{exp,M1}$, is of the unknown sample only. The second experimental measurement, $S_{21}^{exp,M2}$, is the sample backed by a piece of acrylic with a known thickness ℓ_{acr} and constitutive parameters ϵ_r^{acr} and μ_r^{acr}. Acrylic is a lossless dielectric having a relative permeability, $\mu_r = 1 + j0$. This fact leads to a fundamental frequency phenomenon when the phase of a single-layer material given by $P = e^{-jk_{z_o}\ell_{acr}}$ is equal to a multiple of a half wavelength. At the fundamental frequency when $m = 1$ there is no phase difference and very little magnitude difference between the two measurements. The phase term is determined by the waveguide propagation constant and the thickness of the acrylic sample

$$\theta = k_{z_o}\ell_{acr} \tag{3.2}$$

where

$$k_{z_o} = \sqrt{k_o^2 \varepsilon_r^{acr} \mu_r^{acr} - k_c^2} \tag{3.3}$$

The free-space propagation constant k_o is given by

$$k_o^2 = \omega^2 \varepsilon_o \mu_o \tag{3.4}$$

substituting into (3.3) along with angular frequency $\omega = 2\pi f$ results in the following

$$k_{z_o} = \sqrt{(2\pi f)^2 \varepsilon_o \mu_o \varepsilon_r^{acr} \mu_r^{acr} - k_c^2} \tag{3.5}$$

The above equation for the waveguide propagation constant is substituted into (3.2)

$$k_{z_o} = \left(\sqrt{(2\pi f)^2 \varepsilon_o \mu_o \varepsilon_r^{acr} \mu_r^{acr} - k_c^2} \right) \ell_{acr} = m\pi \tag{3.6}$$

solving for f_o results in the following expression for the fundamental waveguide frequency

$$f_o = \sqrt{\frac{\frac{\pi^2}{\ell_{acr}^2} + k_c^2}{4\pi^2 \varepsilon_o \mu_o \varepsilon_r^{acr} \mu_r^{acr}}} \tag{3.7}$$

Setting k_c, the waveguide cutoff frequency, equal to zero and applying the definition of the speed of light in free-space

$$c \equiv \frac{1}{\sqrt{\varepsilon_o \mu_o}} \tag{3.8}$$

(3.7) simplifies to the fundamental free-space frequency given below

$$f_0 = \frac{c}{2\ell_{acr} \sqrt{\varepsilon_r^{acr} \mu_r^{acr}}} \tag{3.9}$$

At the fundamental frequency the 2D root search will not converge to a solution. To ensure the two measurements have sufficient differences in phase the thickness of the acrylic is chosen such that $\theta = k_0 \ell \geq 30^\circ$. This value accounts for the phase accuracy of the NWA which is roughly 15° at 18 GHz resulting in a safety margin ensuring

convergence to a solution. A maximum phase value is also chosen in case a reflection measurement is taken in the future. In the case of a reflection measurement the phase is a two-way value and a 180° phase difference will not result in a solution. Therefore, the maximum phase difference is chosen to be $\theta = k_0\ell \leq 150°$ this also includes a safety margin. This phase requirement cannot be satisfied over the entire bandwidth of the focus arch system (2-18 GHz) using a single piece of acrylic. Therefore, the band is broken into two smaller bandwidths ranging from 2-6 GHz and 6-18 GHz requiring two pieces of acrylic. The thickness is required to be $\frac{\lambda}{4}$ at mid-band to ensure optimum incident power across the entire band. This requirement also helps ensure that the phase across the band does not approach 0° or 180°. The wavelength λ in a rectangular waveguide is given by the following equation

$$\lambda = \frac{2\pi}{k_{z_o}} \tag{3.10}$$

Substituting (3.5) from above into (3.10) results in the below equation for wavelength

$$\lambda = \frac{2\pi}{\sqrt{(2\pi f)^2 \varepsilon_o \mu_o \varepsilon_r^{acr} \mu_r^{acr} - k_c^2}} \tag{3.11}$$

Requiring $\ell_{acr} = \frac{\lambda}{4}$ and solving (3.11) for the acrylic thickness at the mid band frequency f_{mid} gives the following

$$\ell_{f_{mid}}^{acr} = \frac{2\pi}{4\sqrt{(2\pi f_{mid})^2 \varepsilon_o \mu_o \varepsilon_r^{acr} \mu_r^{acr} - k_c^2}} \tag{3.12}$$

As before setting $k_c = 0$ and applying the definition of the speed of light in free-space simplifies (3.12) to give the acrylic thickness at the mid band frequency for free-space shown below

$$\ell_{f_{mid}}^{acr} = \frac{c}{4 f_{mid} \sqrt{\varepsilon_r^{acr} \mu_r^{acr}}} \tag{3.13}$$

The acrylic thickness required at $f_{mid} = 4$ GHz and $f_{mid} = 12$ GHz is .453" and .151", respectively. Commercially available sizes of .5" and .125" are chosen to reduce cost. The minimum and maximum phase across the band is verified using (3.2).

Substituting (3.5) into (3.2) leads to the equation for the waveguide phase at the minimum and maximum frequencies $f_{min,max}$ of the band

$$\theta = \left(\sqrt{(2\pi f_{min,max})^2 \varepsilon_o \mu_o \varepsilon_r^{acr} \mu_r^{acr} - k_c^2} \right) \ell_{acr} \tag{3.14}$$

Setting $k_c = 0$ and applying the definition of the speed of light in free-space simplifies (3.14) to give the minimum and maximum free-space phase

$$\theta = \frac{2\pi f_{min,max} \ell^{acr} \sqrt{\varepsilon_r \mu_r}}{c} \tag{3.15}$$

For the .5" acrylic sample the phase across the band ranges from $45.6° \leq \theta \leq 137.1°$ and for the .125" sample the phase ranges from $34.3° \leq \theta \leq 102.8°$. The phase difference for both waveguide systems can be easily satisfied using the above acrylic thicknesses.

3.2 Waveguide

Both S-band (2.6-3.95 GHz) and X-band (8.2-12.4 GHz) rectangular waveguides are used to demonstrate the transmission technique. Figure 3.1(a) shows the S-band waveguide including the measured samples and the sample holder. The cutoff wave number for the S-band waveguide is given by

$$k_c = \frac{\pi}{a} \tag{3.16}$$

where a is the longest dimension of the waveguide, for S-band $a = .072136$ m. The X-band waveguide, measured samples, and sample holder are shown in Figure 3.1(b) whose longest dimension is $a = .02286$ m.

3.2.1 Calibration. Before taking any measurements it is necessary to calibrate the waveguide system to remove any system errors and establish the phase reference point. This $Z = 0$ phase reference plane is the location of the front face of

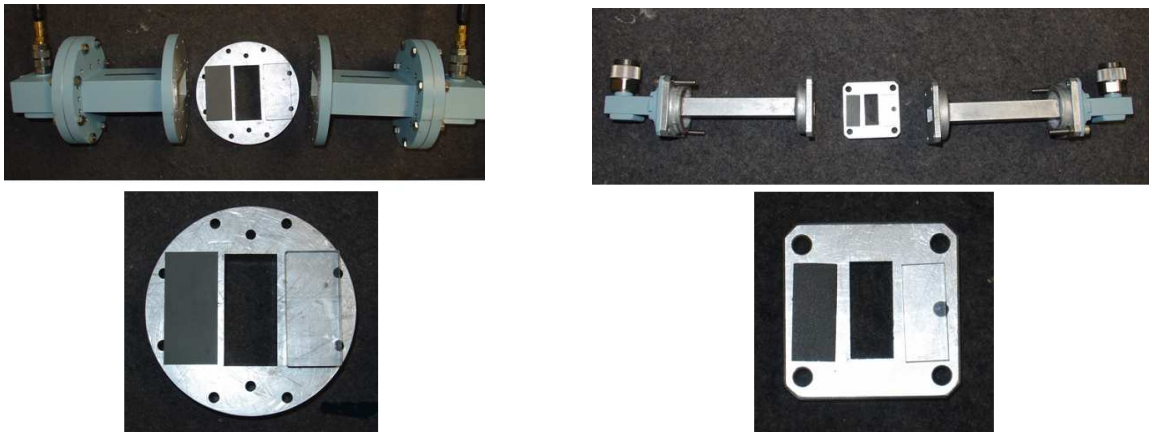

(a) (b)

Figure 3.1: (a) S-band (2.6-3.95 GHz) rectangular waveguide shown with MRAM sample, acrylic sample, and sample holder.
(b) X-band (8.2-12.4 GHZ) rectangular waveguide shown with MRAM sample, acrylic sample, and sample holder.

the sample. The sample will be located at this location for all measurements to ensure the phase delay term is calculated correctly. Figure 3.2 shows the three calibration measurements necessary to calibrate the waveguide system. The HP8510 NWA must be setup prior to calibration. For S-band measurements the start frequency 2.6 GHz and stop frequency 3.95 GHz are set along with the waveguide cutoff frequency (referred to as waveguide delay in the NWA) of 2.078 GHz. Similarly, for the X-band measurements the start frequency 8.2 GHz and stop frequency 12.4 GHz are set along with the waveguide cutoff frequency of 6.557 GHz. The following settings are common between both waveguide systems. The NWA is set to measure 201 frequency points with a 100 ms sweep time taking 64 averages at each frequency. Once the NWA parameters are set the TRL calibration is conducted using a zero delay for the sample holder. This zero delay accommodates the holder for the measurement eliminating the need to take the length of the holder into account. The delay for the S-band and X-band line standards are -32.376 ps and -101.53 ps, respectively. The first calibration measurement is the thru measurement with the sample holder attached. The next calibration measurement is the reflect, made by inserting a short as depicted in Figure 3.2. The final calibration measurement is the line measurement made by

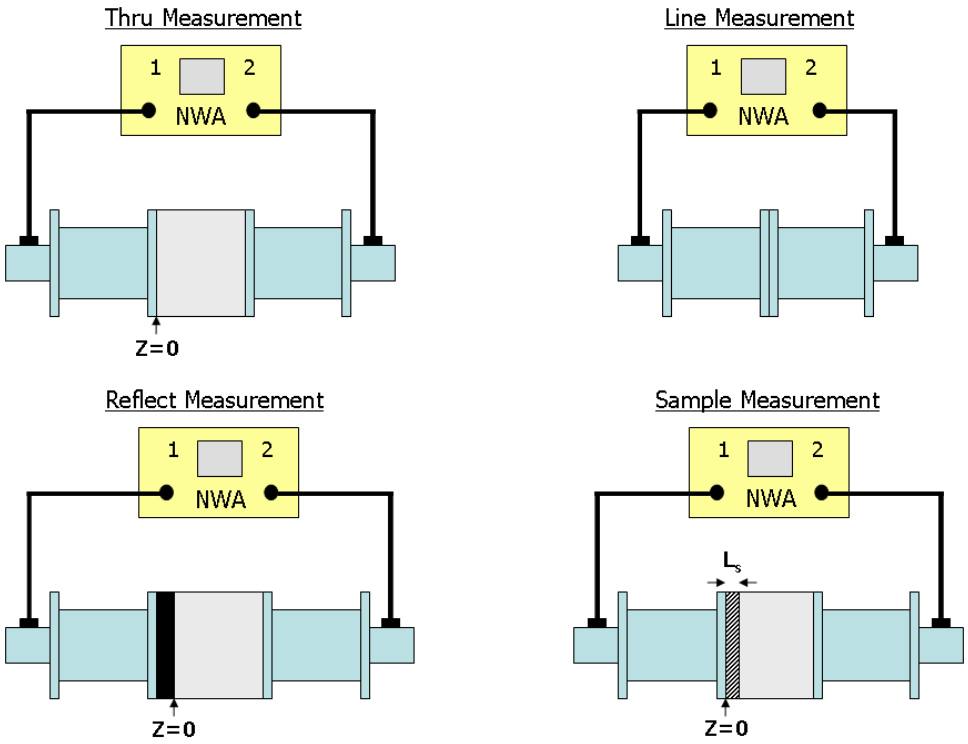

Figure 3.2: Depiction of the calibration setup used for both S-band and X-band waveguide TRL calibration.

connecting the waveguide without the sample holder. After omitting the isolation calibration measurement and saving the calibration coefficients, it is good practice to measure S_{11} to ensure it has a magnitude of one and a phase of 180°.

3.2.2 Waveguide NRW Method. The sample is cut to fill the entire waveguide holder to ensure dominant mode operation. Forward reflection $S_{11}^{exp,meas1}$, and transmission $S_{21}^{exp,meas1}$ S-parameters are measured and recorded. Prior to parameter extraction the measured S-parameters must be phase shifted to account for the thickness of the sample because it is absent in the thru measurement as shown in Figure 3.3(a). The S-parameters are shifted using the below equations

$$\begin{aligned} S_{11}^{exp,M1} &= S_{11}^{exp,meas1} \\ S_{21}^{exp,M2} &= S_{21}^{exp,meas2} e^{-jk_{z_o}\ell_s} \end{aligned} \tag{3.17}$$

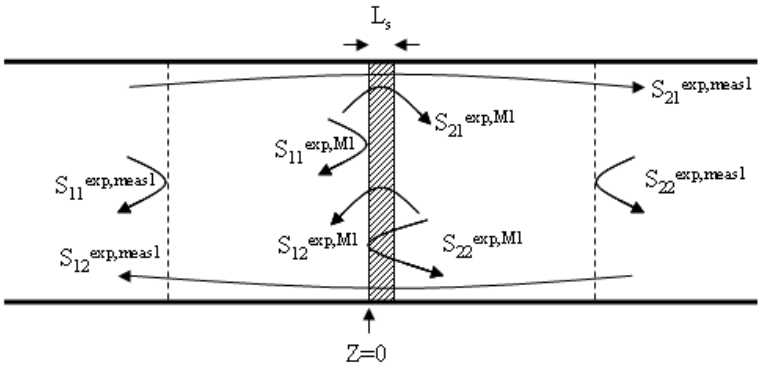

(a)

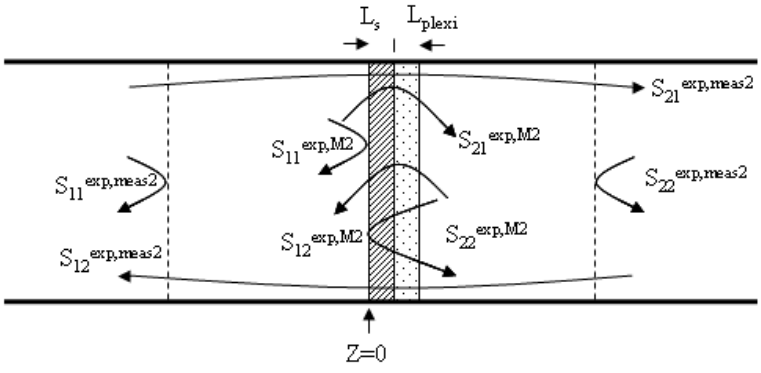

(b)

Figure 3.3: (a) Depiction of phase relationship between measured S-parameters and measured sample S-parameters for a single-layer system.
(b) Depiction of phase relationship between measured S-parameters and measured sample S-parameters for a two-layer system.

where k_{z_o} is the propagation constant and ℓ_s is the sample thickness. The above experimental S-parameters are used in the NRW algorithm outlined in Chapter 2 to extract ϵ_r and μ_r. The extracted complex relative permittivity $\epsilon_{real} + j\epsilon_{imag}$ and complex relative permeability $\mu_{real} + j\mu_{imag}$ of a MRAM sample in a S-band and X-band rectangular waveguide are presented in chapter four.

3.2.3 Waveguide Two Transmission Method. The two transmission method uses the above single-layer sample measurement, $S_{21}^{exp,meas1}$, and a two-layer acrylic backed sample measurement, $S_{21}^{exp,meas2}$. Measurement one is phase shifted as shown in Figure 3.3(a) while measurement two is phase shifted as shown in Figure 3.3(b).

The S-parameters are shifted using the below equations

$$\begin{aligned} S_{21}^{exp,M1} &= S_{21}^{exp,meas1} e^{-jk_{z_o}\ell_s} \\ S_{21}^{exp,M2} &= S_{21}^{exp,meas2} e^{-jk_{z_o}(\ell_s+\ell_{acr})} \end{aligned} \tag{3.18}$$

where k_{z_o} is the propagation constant, ℓ_s is the sample thickness, and ℓ_{acr} is the acrylic thickness. These experimental values are compared to calculated theoretical values using a 2D Newton root search solving the below equations

$$\begin{aligned} |S_{21}^{thy,M1}(\omega,\epsilon,\mu) - S_{21}^{exp,M1}(\omega)| &< accuracy \\ |S_{21}^{thy,M2}(\omega,\epsilon,\mu) - S_{21}^{exp,M2}(\omega)| &< accuracy \end{aligned} \tag{3.19}$$

An initial guess is made for the unknown sample ϵ_r and μ_r and the root search iteratively approaches a solution that satisfies (3.19) to within a specified accuracy. The theoretical transmission coefficient for the single-layer measurement $S_{21}^{thy,M1}$ is given by 2.10 and shown below

$$S_{21}^{thy,M1} = \frac{P(1-R^2)}{1-R^2P^2} \tag{3.20}$$

where

$$\begin{aligned} R &= \frac{Z_{unk}-Z_o}{Z_{unk}+Z_o} \\ P &= e^{-\gamma_{unk}\ell_s} \\ Z_o &= \frac{j\omega\mu_o}{\gamma_o} \\ \gamma_o &= \sqrt{k_c^2-k_o^2} \\ Z_{unk} &= \frac{j\omega\mu_o\mu_r^{unk}}{\gamma_{unk}} \\ \gamma_{unk} &= \sqrt{k_c^2-k_o^2\mu_r^{unk}\varepsilon_r^{unk}} \end{aligned} \tag{3.21}$$

The theoretical transmission coefficient for the two-layer measurement is found by solving (2.21) for A_{11} and using (2.8) to solve for S_{21}

$$S_{21}^{thy,M2} = \frac{T_1 T_2 T_3}{(P_1^{-1} P_2^{-1} + R_1 R_2 P_1 P_2^{-1}) + (P_1^{-1} R_2 P_2 + R_1 P_1 P_2) R_3} \tag{3.22}$$

where R_i, T_i, and P_i are the reflection coefficient, transmission coefficient, and one-way phase delay for the i^{th} interface. The theoretical transmission coefficient for a rectangular waveguide can be further simplified to the following [7]

$$\begin{aligned} S_{21}^{thy,M2} &= \frac{8 Z_o Z_{unk} Z_{acr}}{e^{\gamma_{acr}\ell_{acr}} (Z_{acr} + Z_o) Y^+ + e^{-\gamma_{acr}\ell_{acr}} (Z_o - Z_{acr}) Y^-} \\ Y^{\pm} &= 2 Z_{unk} Z_{acr} \cos k_{zunk}\ell_s \pm 2j Z_{unk}^2 \sin k_{zunk}\ell_s + 2j Z_o Z_{acr} \sin k_{zunk}\ell_s \pm 2 Z_o Z_{unk} \cos k_{zunk}\ell_s \end{aligned} \tag{3.23}$$

where Z_{unk} is the waveguide impedance of the unknown layer, Z_{acr} is the waveguide impedance of the acrylic layer, and k_{zunk} is the propagation constant in the unknown layer. The extracted complex relative permittivity $\epsilon_{real} + j\epsilon_{imag}$ and complex relative permeability $\mu_{real} + j\mu_{imag}$ of a MRAM sample in a S-band and X-band rectangular waveguide are presented in chapter four.

3.3 Frequency-Domain Focus Arch

The frequency-domain focus arch system, free-space system, consists of a NWA connected to a transmit horn antenna through which a TEM wave is transmitted. The wave passes through a system of dielectric lenses that collimate and focus the energy onto the sample. The wave then passes through or is reflected by the sample and is received by another horn antenna as shown in Figure 3.4. Since the sample size is large relative to wavelength and the lens system focuses the beam to a spot on the sample, it can be approximated as infinite in extent and edge scattering effects can be ignored. Unlike the waveguide procedure which uses a TRL calibration the focus arch system requires a significant amount of postprocessing to calibrate the system. The calibration procedure consists of a simple response calibration and range-gating

Figure 3.4: General Electric's focus arch free-space range with transmit horn on the left and receive horn on the right. The sample holder is not shown but is located in the middle, in place of the calibration cylinder shown.

(time-gating) to calibrate the system. Once calibrated the NRW method and two-transmission root search method are used to extract ϵ_r,μ_r.

3.3.1 Two-Transmission Calibration and Extraction. The two transmission method requires three measurements a single-layer sample measurement $S_{21}^{exp,meas1}$, a two-layer acrylic backed sample measurement $S_{21}^{exp,meas2}$, and an empty measurement $S_{21}^{exp,empty}$. All three measurements are processed the same but for illustrative purposes only $S_{21}^{exp,meas1}$ data is shown. Calibration of the free-space frequency-domain system is conducted by first windowing the $S_{21}^{exp,meas1}$ data shown in Figure 3.5(a). The windowing is necessary due to the finite bandwidth of the measurement. When transformed to the time-domain the dynamic range of the time-domain measurement is limited by hiding low level responses within the higher level sidelobes. Frequency windowing the measured data serves to lower the sidelobes that occur when transformed to the time-domain. The Kaiser-Bessel window with $\beta = 6$ is chosen and reduces the sidelobes 50 Decibels (dB) relative to the peak. The frequency-windowed data is shown in Figure 3.5(b). The windowing function causes a rounding effect of the band edges reducing valid data at the band edges. Once windowed and

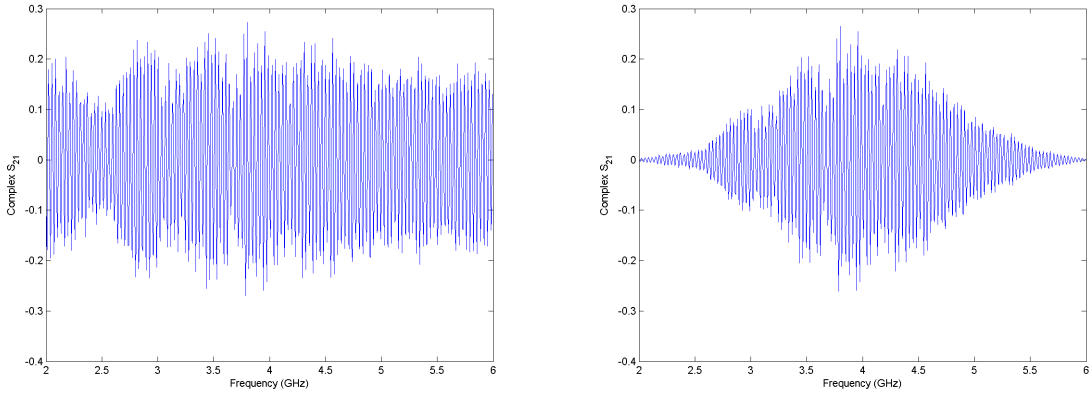

(a) (b)

Figure 3.5: (a) Raw measured forward transmission measurement $S_{21}^{exp,meas1}$ prior to calibration and normalization of a single-layer sample in the focus arch system. (b) Windowed forward transmission measurement.

transformed to the time-domain as shown in Figure 3.6(a) any unwanted interaction between the sample and lens system is gated out. The time gate is applied 1 ns around the location of the sample to ensure lens sample interaction is removed as shown in Figure 3.6(b). After time gating the data is transformed back to the frequency-domain and is normalized to the empty measurement and phase delayed to the $Z = 0$ plane shown in Figure 3.3. The equations for the simple response calibration and phase delay are given by

$$\begin{aligned} S_{21}^{exp,M1} &= \frac{S_{21}^{exp,meas1}}{S_{21}^{exp,empty}} e^{-jk_0\ell_s} \\ S_{21}^{exp,M2} &= \frac{S_{21}^{exp,meas2}}{S_{21}^{exp,empty}} e^{-jk_0(\ell_s+\ell_{acr})} \end{aligned} \tag{3.24}$$

where k_0 is the free-space propagation constant, ℓ_s is the sample thickness, ℓ_{acr} is the acrylic thickness, and $S_{21}^{exp,empty}$ is the forward transmission measurement with no sample in the holder. The resulting calibrated data shown in Figure 3.7 is used in a 2D root search that compare experimental values to the calculated theoretical values using (3.19). The extracted complex relative permittivity $\epsilon_{real} + j\epsilon_{imag}$ and complex

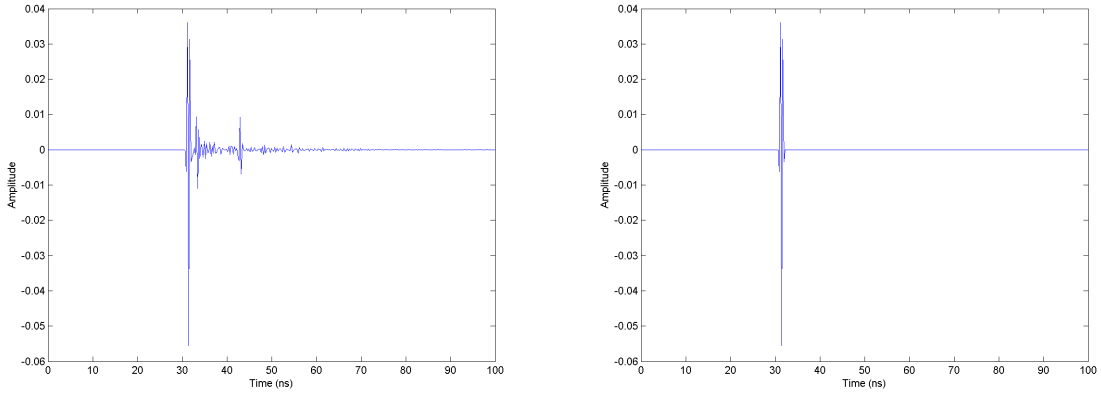

(a) (b)

Figure 3.6: (a) Results of IDFT on windowed forward transmission measurement. (b) Gated time-domain forward transmission measurement.

relative permeability $\mu_{real} + j\mu_{imag}$ of a MRAM sample in a focus arch system are presented in chapter four.

3.3.2 NRW Calibration and Extraction. Unlike the two transmission method the NRW extraction method requires four measurements a short reflection $S_{11}^{exp,short}$, empty transmission $S_{21}^{exp,empty}$, sample reflection $S_{11}^{exp,sample}$, and sample transmission $S_{21}^{exp,sample}$ measurement. The four measurements are processed as stated above to remove any sample lens interactions. A simple response calibration and phase delay is applied given by

$$\begin{aligned} S_{11}^{exp} &= -\frac{S_{11}^{exp,sample}}{S_{11}^{exp,short}} \\ S_{21}^{exp} &= \frac{S_{21}^{exp,sample}}{S_{21}^{exp,empty}} e^{-jk_0(\ell_s+\ell_{acr})} \end{aligned} \tag{3.25}$$

The above calibrated experimental S-parameters are used in the NRW algorithm outlined in Chapter 2 to extract ϵ_r,μ_r. The extracted complex relative permittivity $\epsilon_{real} + j\epsilon_{imag}$ and complex relative permeability $\mu_{real} + j\mu_{imag}$ of a MRAM sample in a focus arch system are presented and compared to the two transmission method in chapter four.

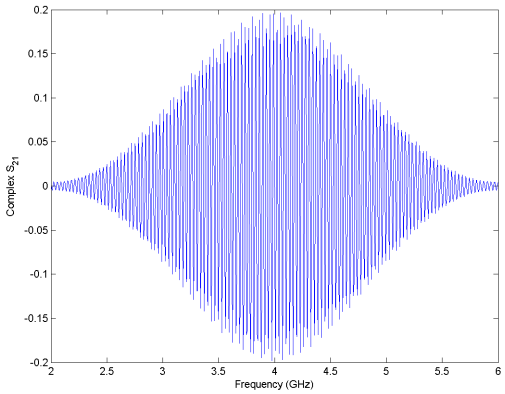

Figure 3.7: Depiction of focus arch system for a single-layer system.

3.4 Direct Time-Domain Focus Arch

The time-domain focus arch, free-space system, consists of an Agilent 86100B digital oscilloscope with 54754A differential time-domain transmission (TDT) module connected to a power amplifier that is connected to a transmit horn antenna. The TDT module within the Oscilloscope creates a 200 mV step with a 40 ps rise time as shown in Figure 3.9. The antenna removes any DC component from the step input and transmits all frequencies within the spectral content of the step input. Unlike the frequency-domain focus arch system the calibration procedure is simplified eliminating the frequency window and transformation to the time-domain steps. The use of direct time-domain measurements serves to increase the band edge data by not requiring a window function. Once calibrated the two-transmission root search method is used to extract ϵ_r and μ_r. The NRW algorithm is not used to extract constitutive parameters in the case of the time-domain free-space system due to the difficulty in taking a reflection measurement. Due to the low output voltage of the TDR/TDT module the antenna acts as a reactive load and does not allow enough energy to propagate and a received signal cannot be measured. With the use of a power amplifier the antenna is able to propagate a measurable signal. However, the use of a power amplifier causes difficulty in making a reflection measurement. A power divider and an additional cable is needed to receive a reflection signal. Additionally, a time delay occurs between the

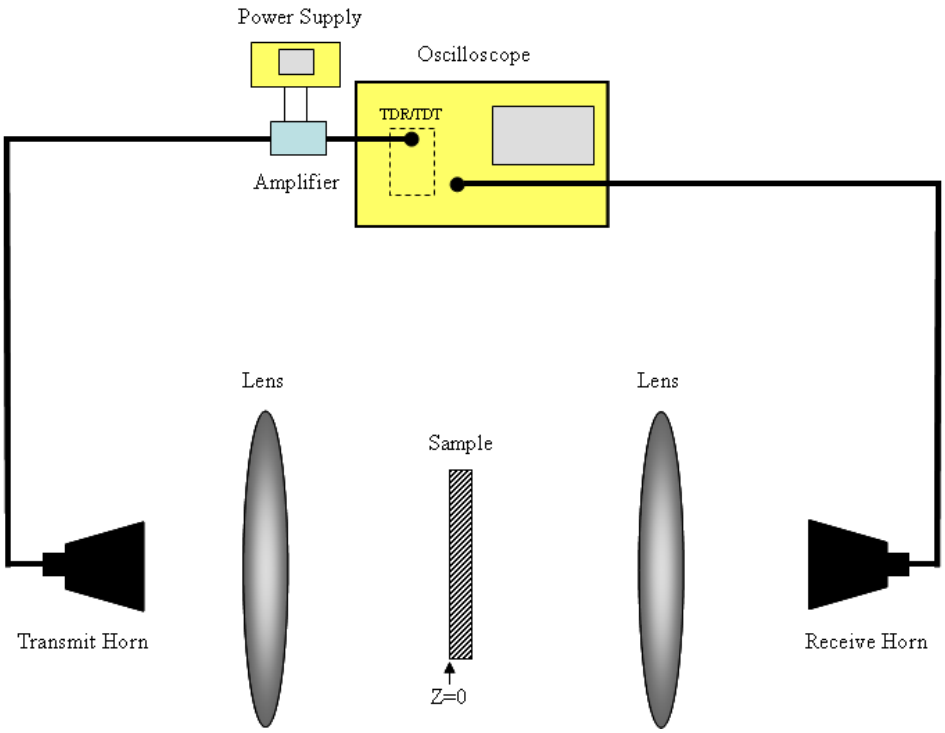

Figure 3.8: Depiction of time-domain focus arch system using a digital oscilloscope with TDR/TDT module connected to a power amplifier.

reflection and transmission measurement due to the power divider and must also be taken into account to ensure correct phase calculation. A reflection measurement can be made with the time-domain system, particularly in systems that do not require an amplifier. However, time-domain reflection measurements in a focus arch free-space system are difficult and are omitted in this thesis.

3.4.1 Two-Transmission Calibration and Extraction. The time-domain two transmission method requires three measurements a single-layer sample measurement $V(t)_{21}^{exp,meas1}$, a two-layer acrylic backed sample measurement $V(t)_{21}^{exp,meas2}$, and an empty measurement $V(t)_{21}^{exp,empty}$. All three measurements are processed the same but for illustrative purposes only $V(t)_{21}^{exp,meas1}$ data is shown. Calibration of the free-space time-domain system is conducted by first time gating the $V(t)_{21}^{exp,meas1}$ measured data shown in Figure 3.10(a). It should be noted that the derivative of the measured

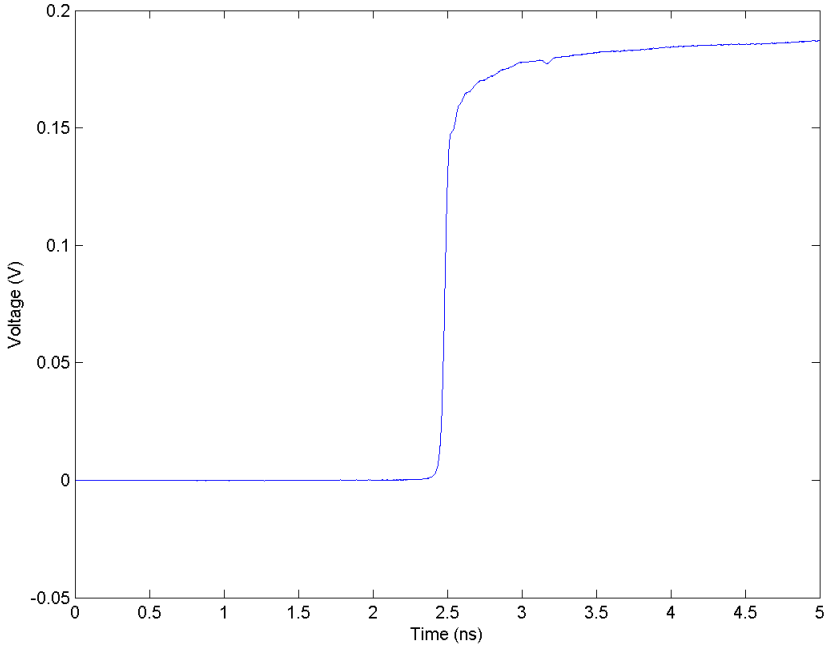

Figure 3.9: Digital oscilloscope TDT module output showing the 200 mV step with a 40 ps rise time.

data may need to be taken prior to time gating when a DC component is present. For instance when using a stripline device the derivative of the step response must be taken to remove the DC component allowing for easier time-gating. Due to the nature of the focus arch system, the DC component is removed by the antenna and the derivative is not necessary. Time gating becomes much more of an art than a science in this case. For the focus arch system the time gating is applied at a zero point in the step response. If the gate is applied at a non-zero point a rounding of the data at the band edges can occur. To ensure valid data across the entire band the time gate must end at a zero crossing as shown in Figure 3.10(b). Once time gated the data is transformed to the frequency-domain and a simple response calibration

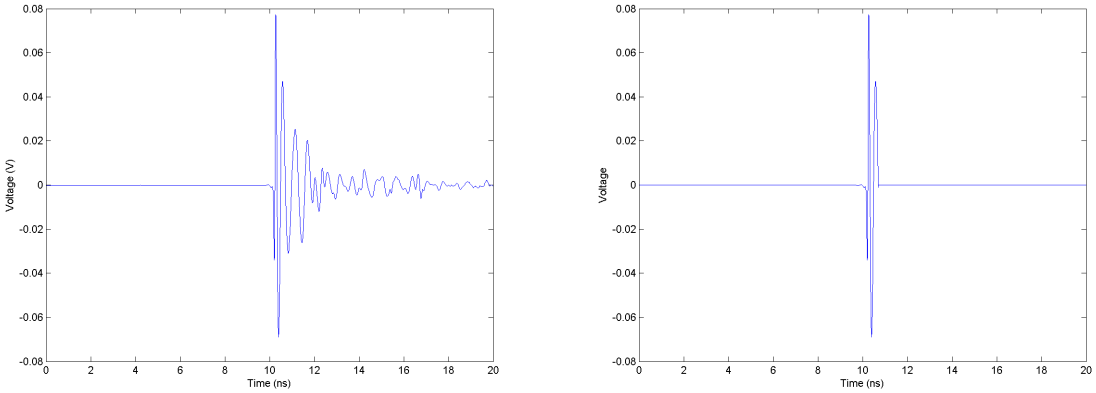

(a) (b)

Figure 3.10: (a) Raw measured forward voltage measurement $V(t)_{21}^{exp,meas1}$ using oscilloscope prior to calibration of a single-layer sample in time-domain focus arch system.
(b) Time gated forward voltage measurement $V(t)_{21}^{exp,meas1}$ prior to calibration of a single-layer sample in time-domain focus arch system.

and phase delay is applied given by

$$\begin{aligned} S_{21}^{exp,M1} &= \frac{S_{21}^{exp,meas1}}{S_{21}^{exp,empty}} e^{-jk_0\ell_s} \\ S_{21}^{exp,M2} &= \frac{S_{21}^{exp,meas2}}{S_{21}^{exp,empty}} e^{-jk_0(\ell_s+\ell_{acr})} \end{aligned} \tag{3.26}$$

where the transmission S-parameter is

$$\begin{aligned} S_{21}^{exp,meas1} &= \frac{V(\omega)^{trans,meas1}}{V(\omega)^{inc}} \\ S_{21}^{exp,meas2} &= \frac{V(\omega)^{trans,meas2}}{V(\omega)^{inc}} \\ S_{21}^{exp,empty} &= \frac{V(\omega)^{trans,empty}}{V(\omega)^{inc}} \end{aligned} \tag{3.27}$$

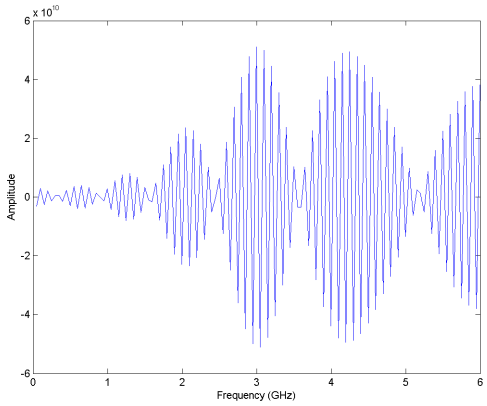

Figure 3.11: Calibrated experimental S-parameters used in 2D Newton root search to extract ϵ_r and μ_r.

resulting in

$$\begin{aligned} S_{21}^{exp,M1} &= \frac{V(\omega)^{trans,meas1}}{V(\omega)^{trans,empty}} e^{-jk_0\ell_s} \\ S_{21}^{exp,M2} &= \frac{V(\omega)^{trans,meas2}}{V(\omega)^{trans,empty}} e^{-jk_0(\ell_s+\ell_{acr})} \end{aligned} \tag{3.28}$$

As shown in (3.28) the incident voltage cancels out and a step or impulse input can be used. The above calibrated experimental S-parameters shown in Figure 3.11 are used in the 2D Newton root search to extract ϵ_r and μ_r. The extracted complex relative permittivity $\epsilon_{real} + j\epsilon_{imag}$ and complex relative permeability $\mu_{real} + j\mu_{imag}$ of a MRAM sample in a time-domain focus arch system are presented and compared to the frequency-domain focus arch results in chapter four.

IV. Results and Analysis

This chapter presents the results of the two transmission method for a rectangular waveguide system, frequency-domain focus arch measurement system, and a time-domain focus arch measurement system. The complex permittivity and permeability of a 40 mil FGM-40 MRAM sample are presented along with a differential uncertainty analysis. The sample is cut to fill the entire cross sectional area of the waveguides and the free-space sample is a 12 in square. The two transmission method can be applied to non-magnetic materials. A 2D root search is not necessary for non-magnetic materials however, the two transmission method can be used and the results for a 125 mil Electric Radar Absorbing Material(ERAM)sample are presented in Appendix A.

4.1 Waveguide System

4.1.1 Uncertainty analysis. Uncertainties in the experimental S-parameters will lead to different solutions that satisfy (3.1). There are many sources of error that contribute to the uncertainty in the waveguide measurement of ϵ_r and μ_r. These include alignment errors causing higher order modes, uncertainties in the sample dimensions, and absorption due to imperfectly conducting waveguide walls [4]. Assuming the walls are perfectly conducting and the sample fully fills the cross section of the waveguide. The main sources of uncertainty for the NRW method are the uncertainty of the sample thickness ℓ_{sample} and reflection path length difference x. The main sources of uncertainty for the two transmission method are the uncertainty in the sample thickness ℓ_{sample}, acrylic thickness $\ell_{acrylic}$, and the relative permittivity of the acrylic ϵ_r^{acr}. The sample thickness is varied by $\ell_{sample} = \pm 1\%$ and the path length difference is varied by a nominal value of $x = \pm 5$ mils for the NRW method. For the transmission method the sample thickness, acrylic thickness, and acrylic permittivity are varied by $\pm 1\%$. The 2D root search and NRW method are run with these measurement uncertainties and the bounds are produced as shown in Figure 4.2.

4.1.2 S-band (2.6-3.95 GHz). Figure 4.2 shows the complex permittivity of a MRAM sample using a S-band rectangular waveguide for the forward NRW and

two transmission method. As can be seen from the figure the use of the reflection measurement in the NRW method causes a large uncertainty. The two transmission method is less sensitive to the position of the material and therefore has a much smaller uncertainty and comparable values to the NRW method. Some of the uncertainty in the measurements may be due to the low frequencies and thin sample. The complex permeability of the MRAM sample is shown in Figure 4.3. The results for the S-band rectangular waveguide shows the two transmission method is as good or better than the NRW method with a lower opportunity for uncertainty.

4.1.3 X-band (8.2-12.4 GHz). The complex permittivity of the MRAM sample using a X-band rectangular waveguide for the forward NRW and two transmission methods are shown in Figure 4.4. Similar to the S-band measurements the X-band measurements exhibit a large uncertainty when using the NRW method. This uncertainty is increased in the X-band waveguide due to the higher frequencies. The two transmission method exhibits a much smaller uncertainty and comparable values to the NRW method. The complex permeability of the MRAM sample is shown in Figure 4.5. The results for the X-band rectangular waveguide shows the two transmission method is more accurate measurement method.

4.2 Focus Arch System (2-18 GHz)

4.2.1 Uncertainty analysis. Some of the errors in the free-space system are the collimation and focusing of the beam, sample antenna interactions, and background interference. These errors are predominantly eliminated through the simple response and range gating calibration. The sample thickness and path length difference are the main sources of uncertainty for the NRW method. Sample thickness is varied by $\ell_{sample} = \pm 1\%$ and the path length difference is varied by a nominal value of $x = \pm 10$ mils for the NRW method. The increase in the reflection path length uncertainty is due to the increase in path length and sample size. The path length for the waveguide system is less than a foot whereas the free-space path length is 6 feet

for the free-space system. The waveguide system offers greater accuracy in sample placement. For the transmission method the sample thickness, acrylic thickness, and acrylic permittivity are varied by ±1%. The 2D root search and NRW method are run with these measurement uncertainties and the bounds are produced as shown in Figure 4.6.

4.2.2 Frequency-Domain. Figure 4.6 shows the complex permittivity of a MRAM sample in a focus arch system from 2-6 GHz using the forward NRW and two transmission methods. As can be seen from the figure the use of the reflection measurement in the NRW method causes a slightly larger uncertainty than the two transmission measurements. Both extraction methods compare well with the values found using the waveguide system. Note the band edge roll off that occurs at 2.5 and 5.5 GHz. The complex permeability of the MRAM sample is shown in Figure 4.7. The results for the frequency-domain focus arch system shows the two transmission method has comparable values to the NRW method with lower uncertainty. The complex permittivity of a MRAM sample in a focus arch system from 6-18 GHz using the forward NRW and two transmission methods are shown in Figure 4.8. As can be seen from the figure the use of the reflection measurement in the NRW method causes a much larger uncertainty than the two transmission measurements due to the higher frequencies (smaller wavelengths). Again values for both extraction methods compare well with the values found using the waveguide system. Note the band edge roll off that occurs at 6.5 GHz and 17 GHz due to windowing the frequency data. The complex permeability of the MRAM sample is shown in Figure 4.9. The results at higher frequencies for the frequency-domain focus arch system shows the two transmission method is a more accurate measurement method than the NRW algorithm.

4.2.3 Time-Domain. The complex permittivity of a MRAM sample in a frequency-domain and time-domain focus arch system from 2-6 GHz using the two transmission method are shown in Figure 4.10. The uncertainty in the two measure-

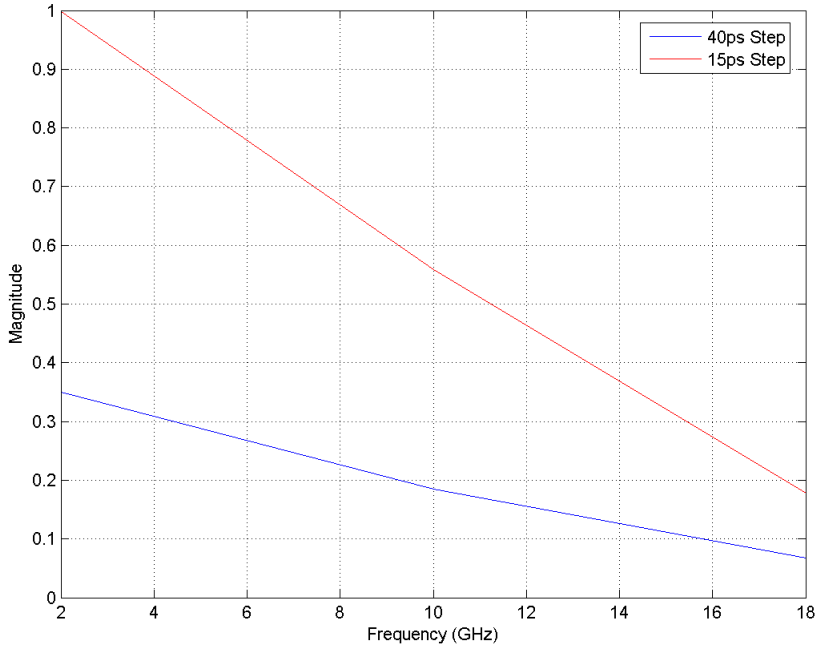

Figure 4.1: Comparison of the normalized spectral content contained in a 40 *ps* step input signal from the TDR/TDT module and a 15 *ps* step input signal from a pulse generator.

ment systems are calculated the same. The real difference between these two methods is the increase in valuable band edge data. The time-domain results hold constant throughout the band while the frequency-domain results diverge at the edges. The complex permeability of the MRAM sample is shown in Figure 4.11. The time-domain results in the lower frequency band is comparable to the frequency-domain results. Figure 4.12 shows the complex permittivity of a MRAM sample in a frequency-domain and time-domain focus arch system from 6-18 GHz using the two transmission method. The complex permeability of the MRAM sample is shown in Figure 4.13. The time-domain measurements increase band edge data as expected. However, at frequencies above 10 GHz the time-domain results diverge from the frequency-domain results. This is due to the limited spectral content of the 40 *ps* rise time step input. To increase accuracies at higher frequencies it will be necessary to increase the rise time of the step input. Figure 4.1 shows the normalized spectral content of the time-domain

system using a 200 mV step input compared to a -5 V 15 ps step input using a pulse generator. Note the decrease in spectral content at higher frequencies resulting from the slow rise time of the step. The magnitude of the spectral content at 10 GHz is half that of the 2 GHz value. Figure 4.1 also shows the increased spectral content achieved by using a faster rise time (fall time) using a pulse generator. Overall the direct time-domain results compare well with the frequency-domain but is most accurate at lower frequencies.

4.2.4 Frequency-Domain and Time-Domain Comparison. Some of the benefits in using the frequency-domain system include a stable signal source, large dynamic range, and lower external interference. Benefits of the time-domain system include easily gating multipath interference, broadband data is obtained in one measurement, and measurements are very rapid. There are also drawbacks to each system. The frequency-domain system requires large averaging, frequency windowing, and transformation to the time-domain is required for gating. The time-domain system requires large averaging to achieve good Signal-to-Noise Ratio (SNR), fast rise-time is required for high spectral content, and it is prone to interference from external sources [5]. The direct time-domain system requires a power amplifier with a fast response time which can be quite costly. The time-domain system also requires additional hardware to achieve higher frequency measurements.

4.3 Summary

The results show that the two transmission method is a valid measurement method for measuring the complex permittivity and permeability of a MRAM sample. Furthermore, the two transmission method has a lower uncertainty than the NRW method especially at higher frequencies. Using the two transmission method in a direct time-domain focus arch system can further increase measurement accuracy by increasing band edge data while decreasing processing time. However, the direct

time-domain system may need additional hardware to achieve accurate high frequency results.

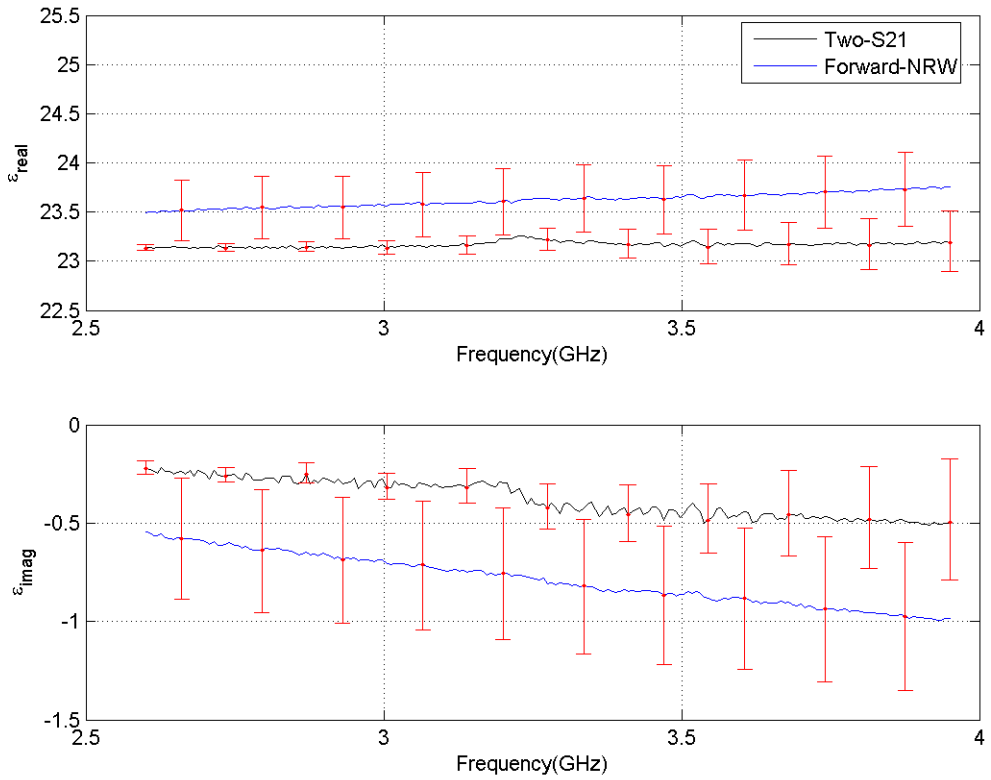

Figure 4.2: Permittivity of MRAM sample using S-band rectangular waveguide for the forward NRW and two transmission method.

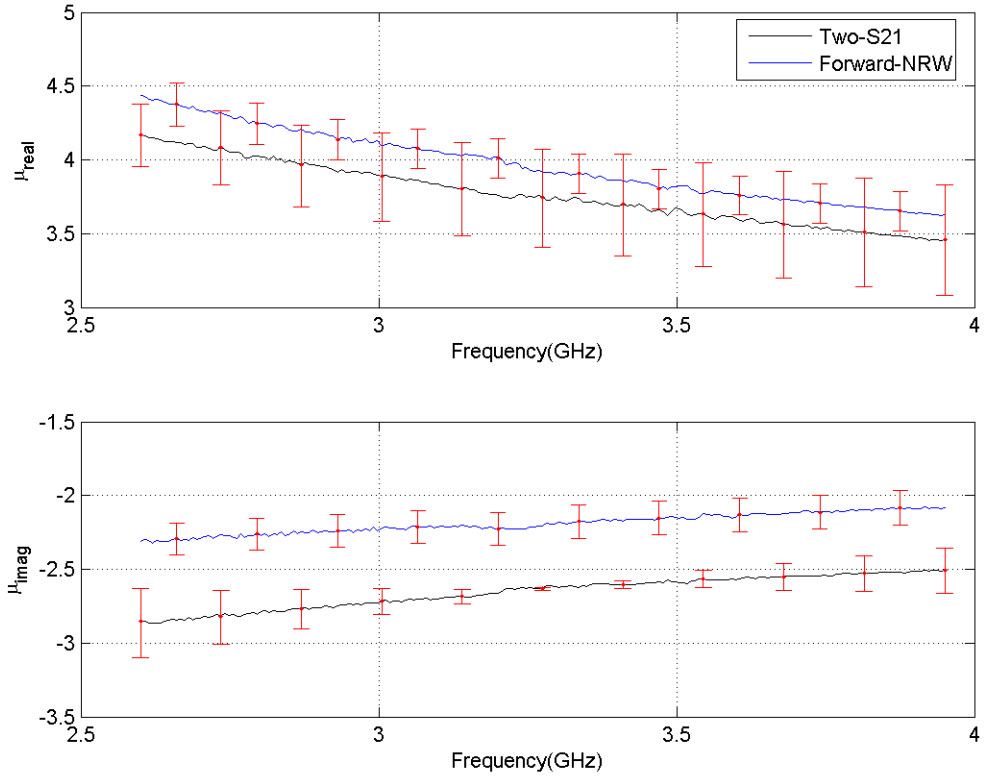

Figure 4.3: Permeability of MRAM sample using X-band rectangular waveguide for the forward NRW and two transmission method.

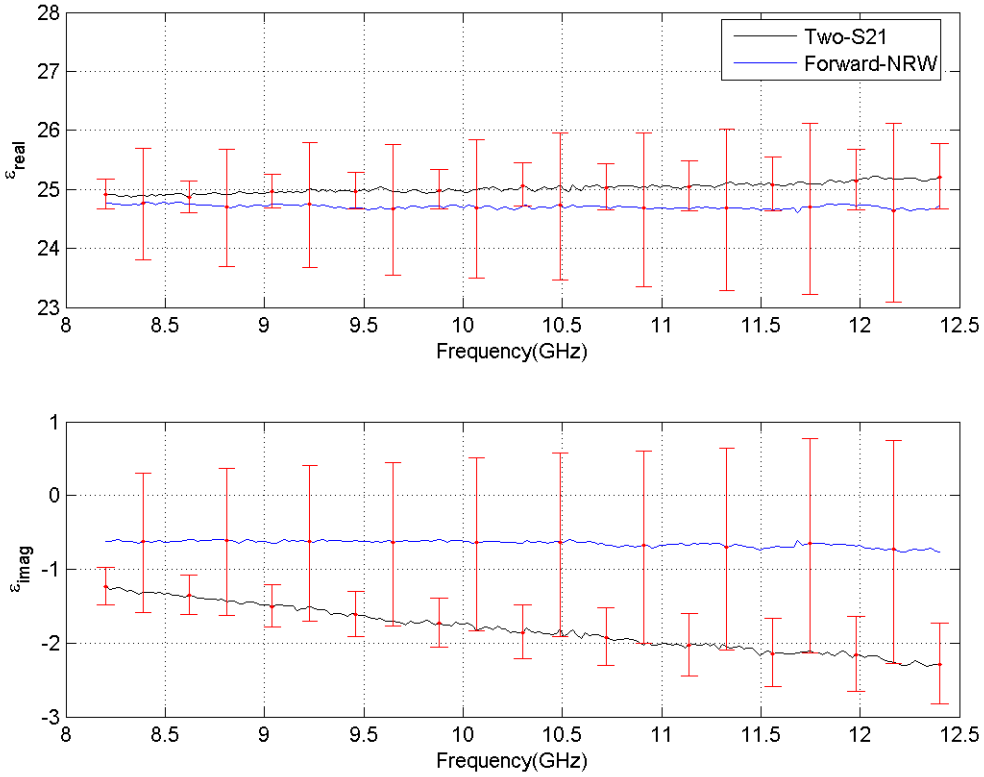

Figure 4.4: Permittivity of MRAM sample using X-band rectangular waveguide for the forward NRW and two transmission method.

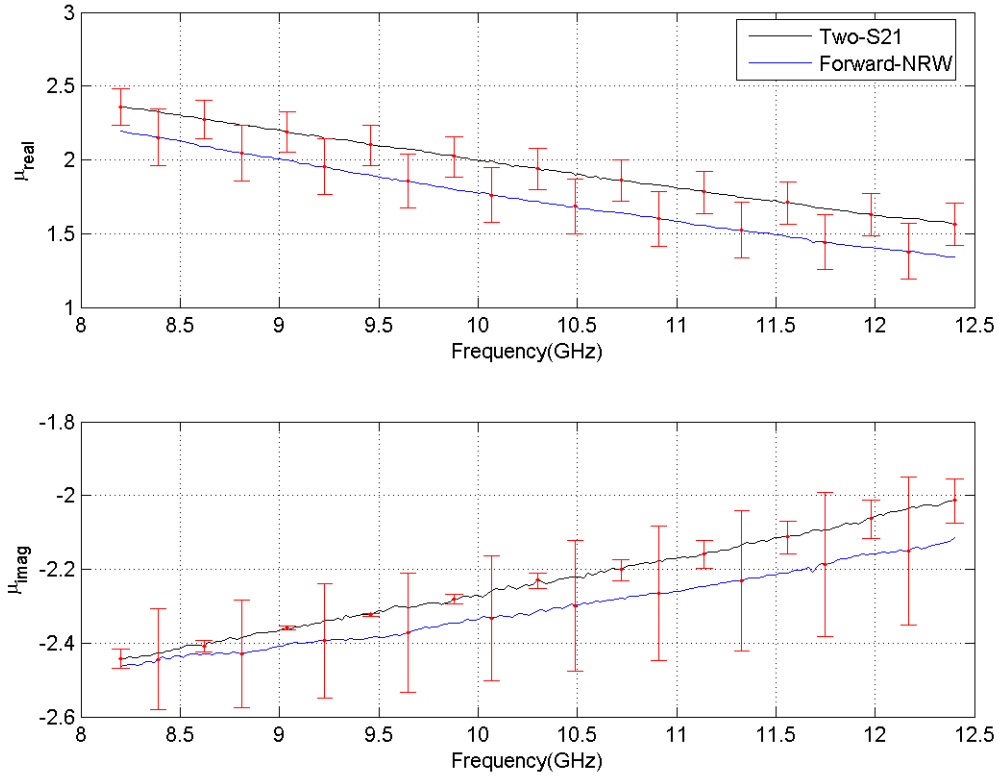

Figure 4.5: Permeability of MRAM sample using X-band rectangular waveguide for the forward NRW and two transmission method.

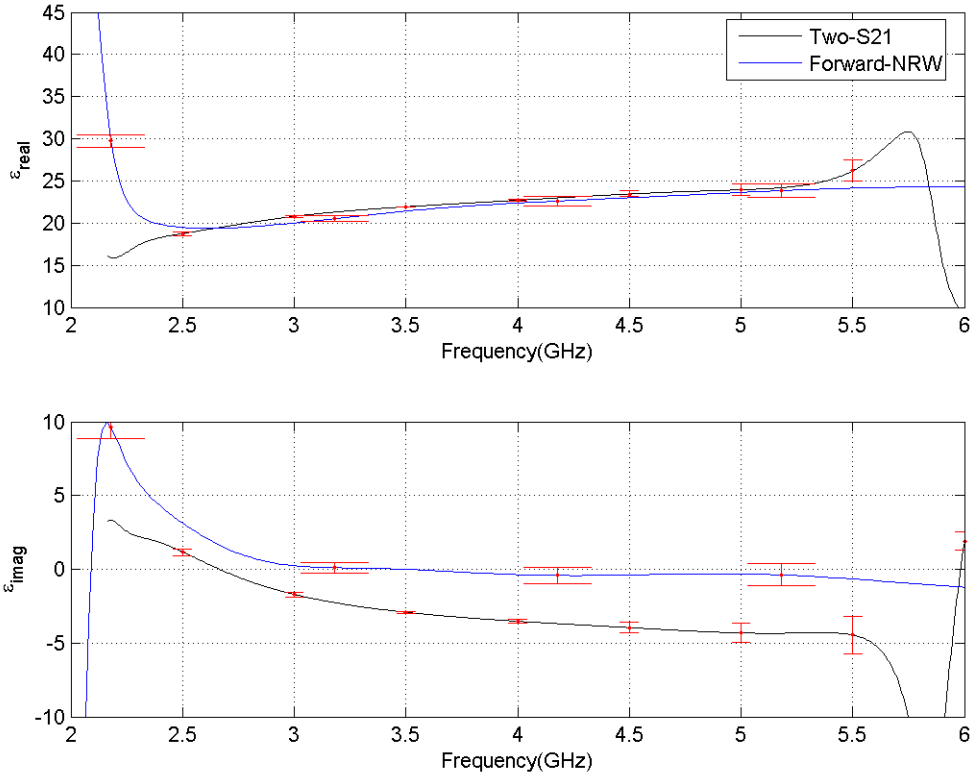

Figure 4.6: Permittivity of MRAM sample measured with the focus arch free-space system from 2-6 GHz for the forward NRW and two transmission method.

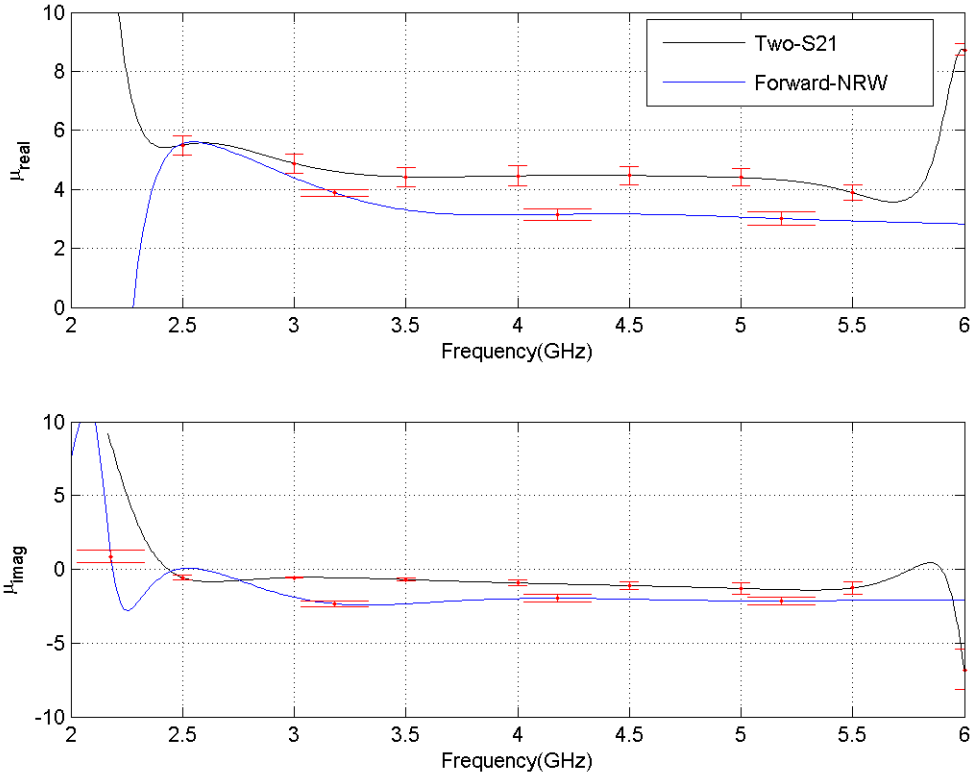

Figure 4.7: Permeability of MRAM sample measured with the focus arch free-space system from 2-6 GHz for the forward NRW and two transmission method.

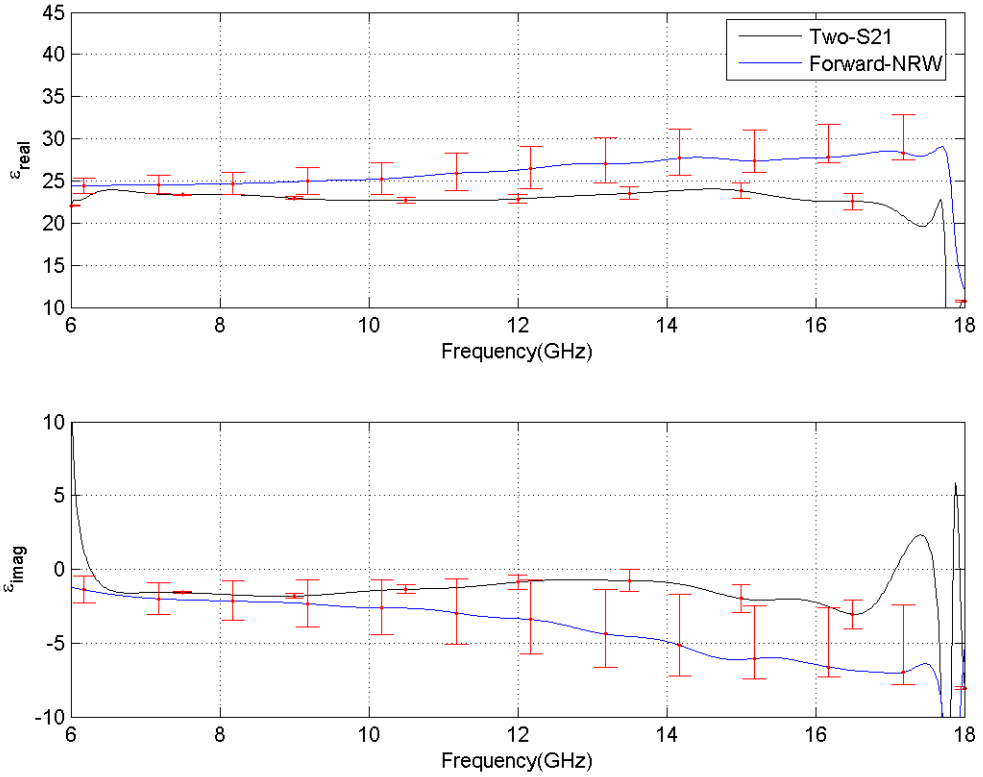

Figure 4.8: Permittivity of MRAM sample measured with the focus arch free-space system from 6-18 GHz for the forward NRW and two transmission method.

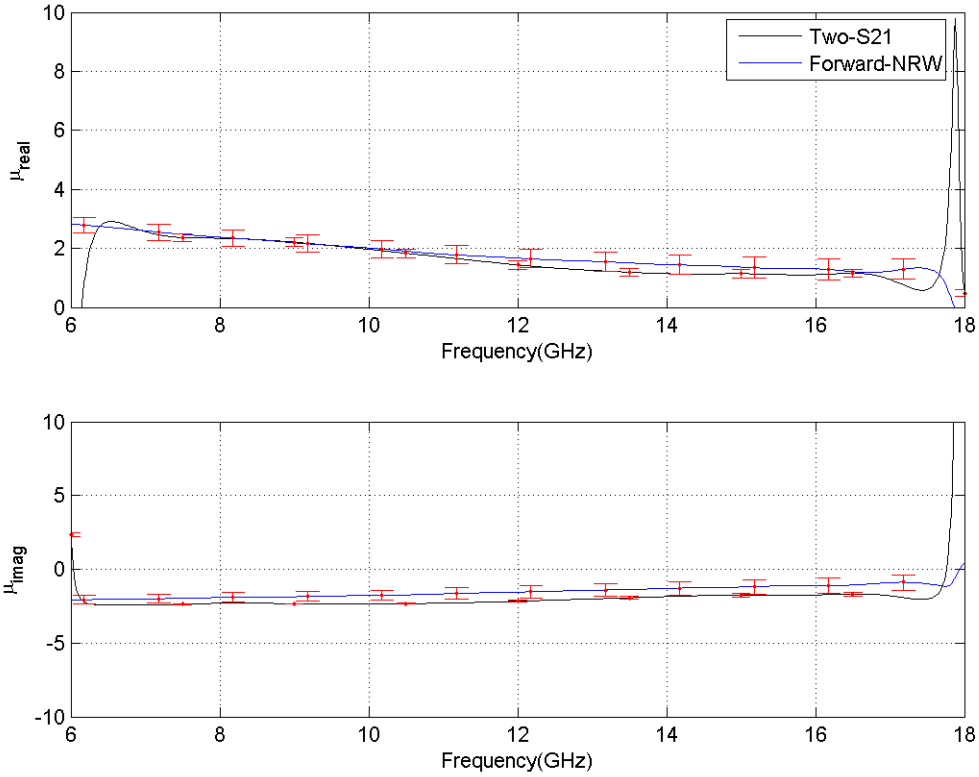

Figure 4.9: Permeability of MRAM sample measured with the focus arch free-space system from 6-18 GHz for the forward NRW and two transmission method.

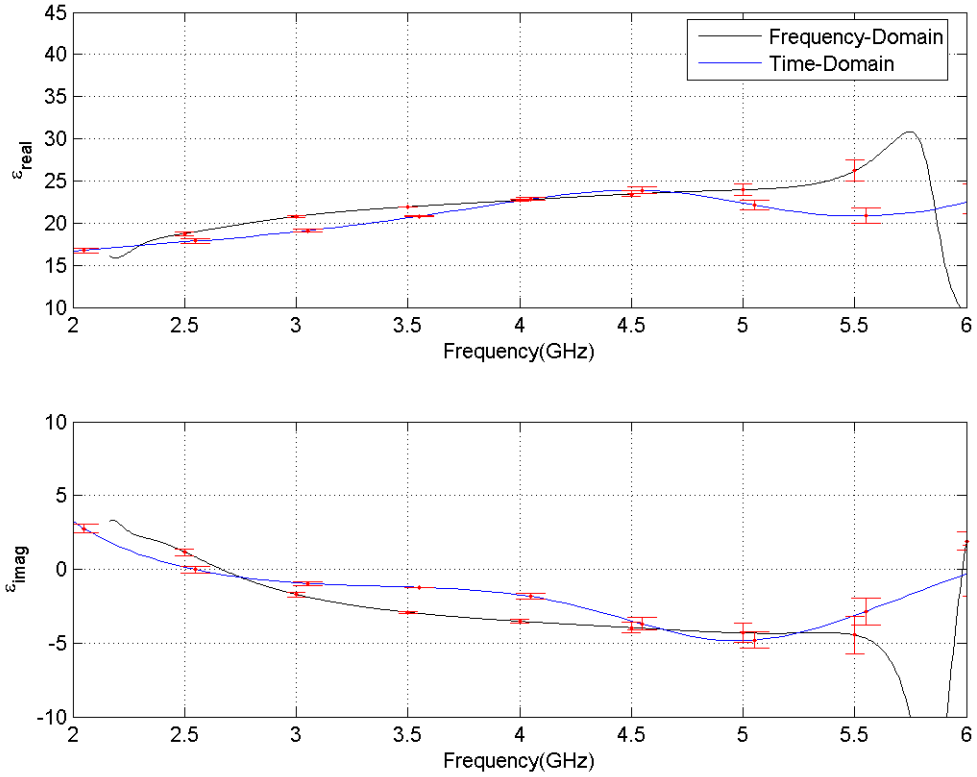

Figure 4.10: Permittivity of MRAM sample measured with the focus arch free-space system from 2-6 GHz for the frequency-domain two transmission method and time-domain two transmission method.

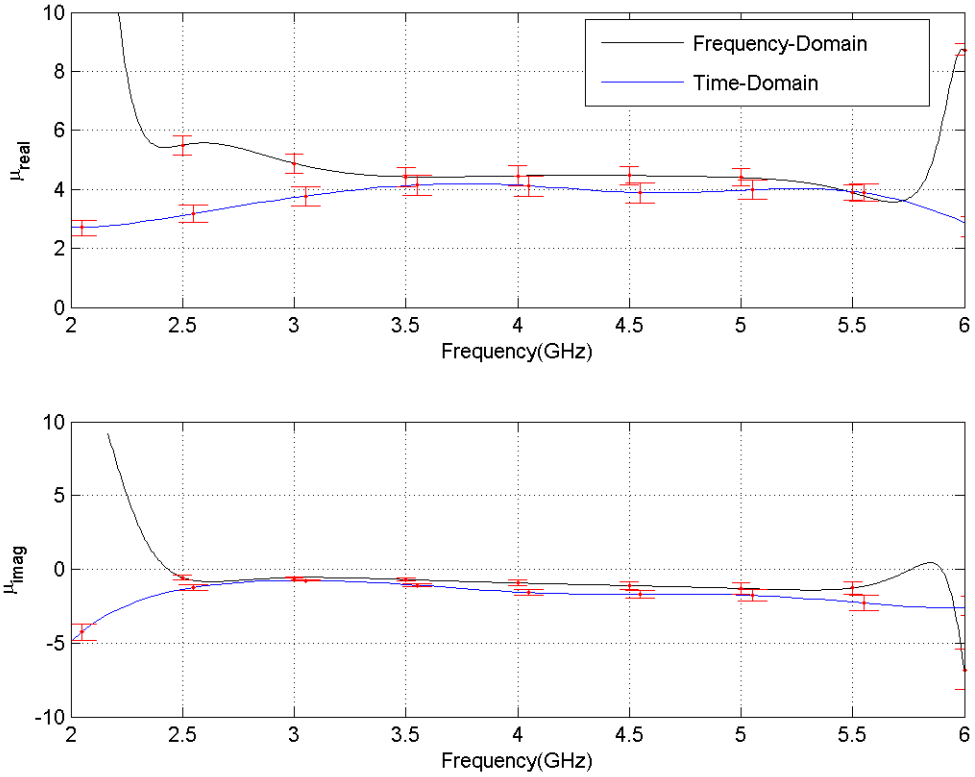

Figure 4.11: Permeability of MRAM sample measured with the focus arch free-space system from 2-6 GHz for the frequency-domain two transmission method and time-domain two transmission method.

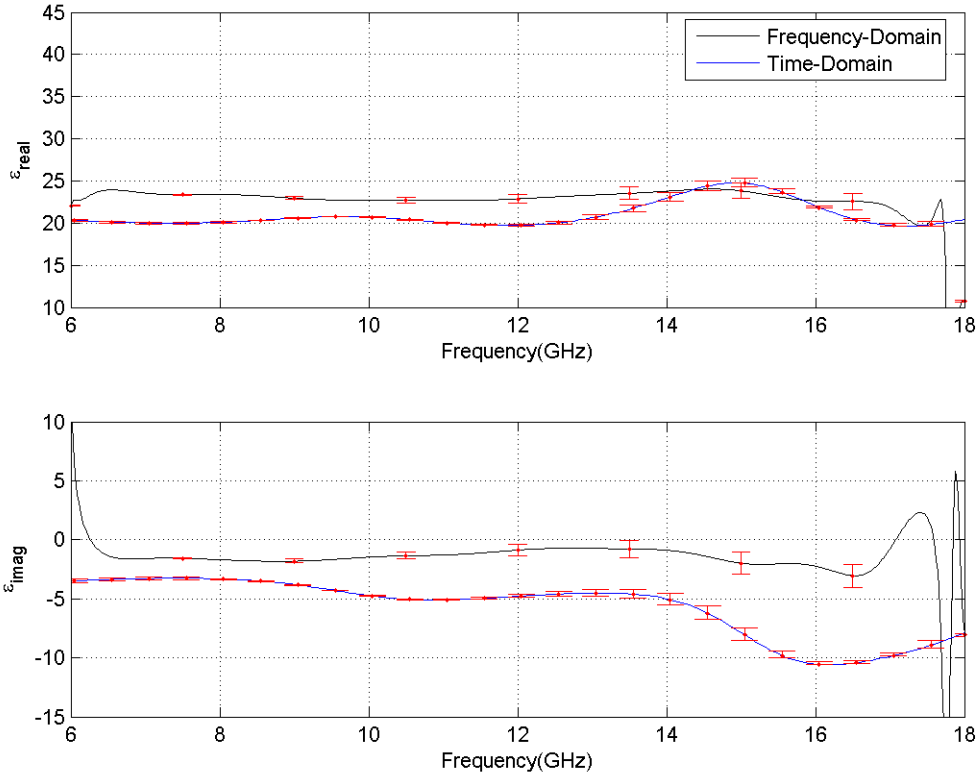

Figure 4.12: Permittivity of MRAM sample measured with the focus arch free-space system from 6-18 GHz for the frequency-domain two transmission method and time-domain two transmission method.

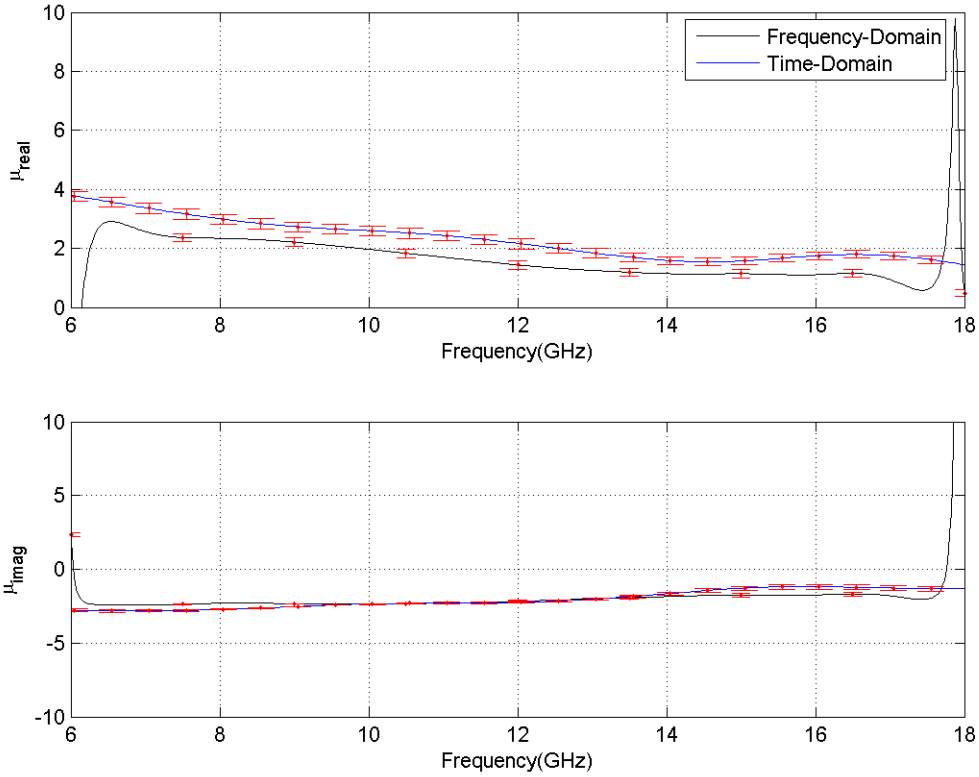

Figure 4.13: Permeability of MRAM sample measured with the focus arch free-space system from 6-18 GHz for the frequency-domain two transmission method and time-domain two transmission method.

V. Conclusions

A two transmission technique was developed to improve constitutive parameter measurements. The permittivity and permeability was extracted using the well known NRW algorithm and are compared to the two transmission technique that extracts permittivity and permeability through the use of a 2D Newton root search.

The technique was first experimentally demonstrated using a MRAM sample in a rectangular waveguide system and compared to the NRW method. The comparisons demonstrated the validity of this method and the improvement over the NRW method. The technique was then extended to a frequency-domain and time-domain focus arch free-space system. A differential uncertainty analysis showed that due to the path length dependence of the reflection measurement the NRW method leads to greater uncertainty. The validity of using a time-domain focus arch system to increase band edge data was demonstrated and compared to the frequency-domain system.

The results of this thesis show the improved measurement accuracy of constitutive parameters using the two transmission method over the NRW method. Also, the use of this technique in a time-domain free-space system slightly improves band edge data while removing two processing operations.

5.1 Future Research

There are a few general improvements that could be made to increase this techniques application to direct time-domain measurements.

5.1.1 Air Gap Error Analysis. A further investigation into the error due to a finite air gap between the sample and acrylic should be conducted. This analysis may show the need to ensure intimate contact between the sample and acrylic. A three-layer analysis using a Newton 2D root search can be conducted similar to the two-layer development of this thesis.

5.1.2 Low Frequency Application. The direct time-domain system has great potential at low frequencies in its current configuration. Low frequency preliminary

measurements have been made using a stripline system. Initial results show improved band edge data compared to the conventional NWA frequency-domain system. The use of the oscilloscope and TDT module should produce improved low frequency material measurements.

5.1.3 High Frequency Application. The direct time-domain system may be used for high frequency applications with additional hardware. The use of a pulse generator and remote pulse head can increase the rise time of the step input. Increasing the rise time will increase spectral content and enable higher frequency applications. High frequency differential time-domain analysis can also be accomplished using Picosecond Pulse Lab's TDR/TDT module. The TDR/TDT module increases the 40 *ps* rise time of the step input to 9 *ps* resulting in much greater spectral content.

Appendix A. ERAM Results

A.1 Waveguide System

A.1.1 S-band (2.6-3.95 GHz).

A.1.2 S-band (8.2-12.4 GHz).

A.2 Waveguide System

A.2.1 Frequency-Domain.

A.2.2 Time-Domain.

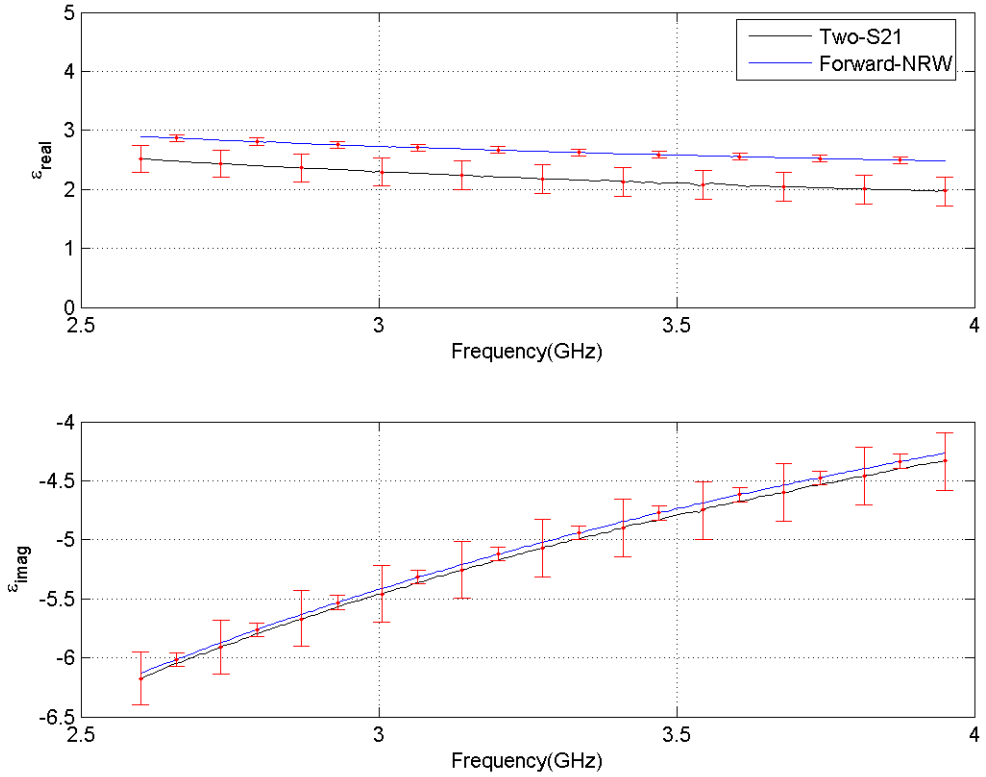

Figure A.1: Complex permittivity of 125 mil ERAM sample measured with the S-band rectangular waveguide system from 2.6-3.95 GHz for the forward NRW and two transmission method.

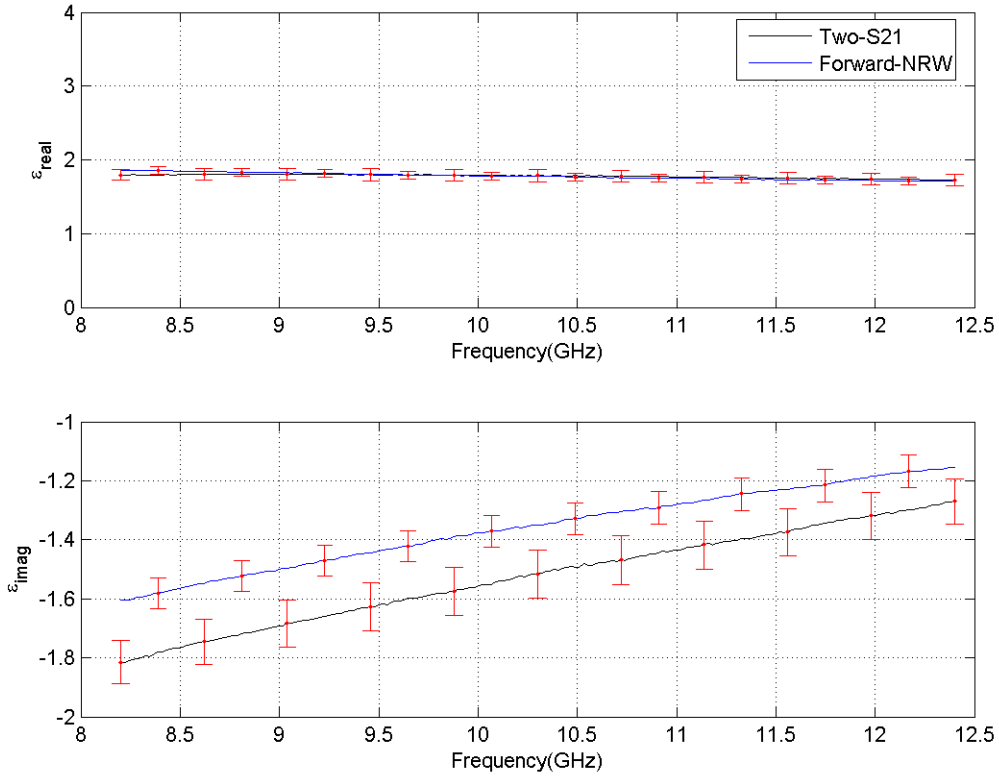

Figure A.2: Complex permittivity of 125 mil ERAM sample measured with the X-band rectangular waveguide system from 8.2-12.4 GHz for the forward NRW and two transmission method.

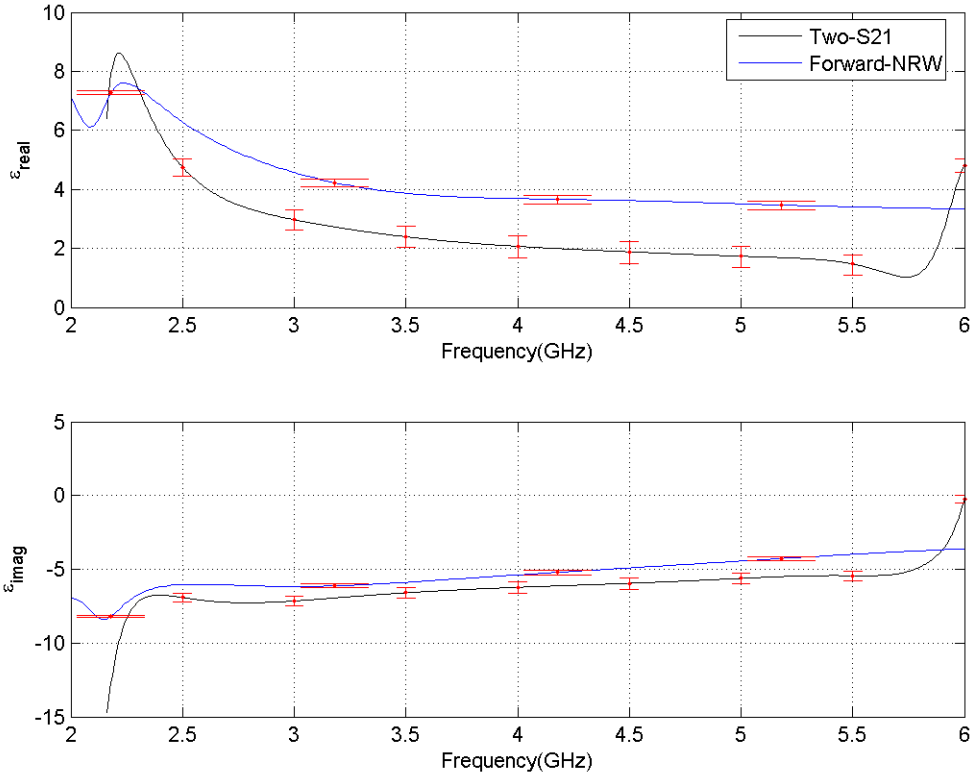

Figure A.3: Complex permittivity of 125 mil ERAM sample measured with the focus arch free-space system from 2-6 GHz for the forward NRW and two transmission method.

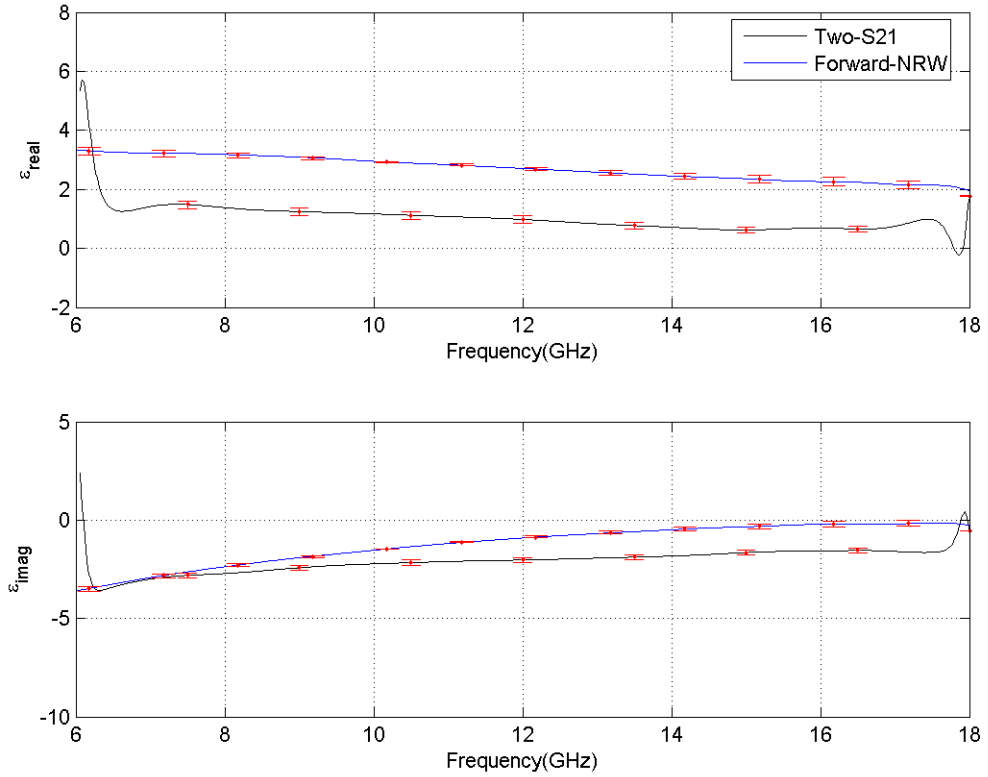

Figure A.4: Complex permittivity of 125 mil ERAM sample measured with the focus arch free-space system from 6-18 GHz for the forward NRW and two transmission method.

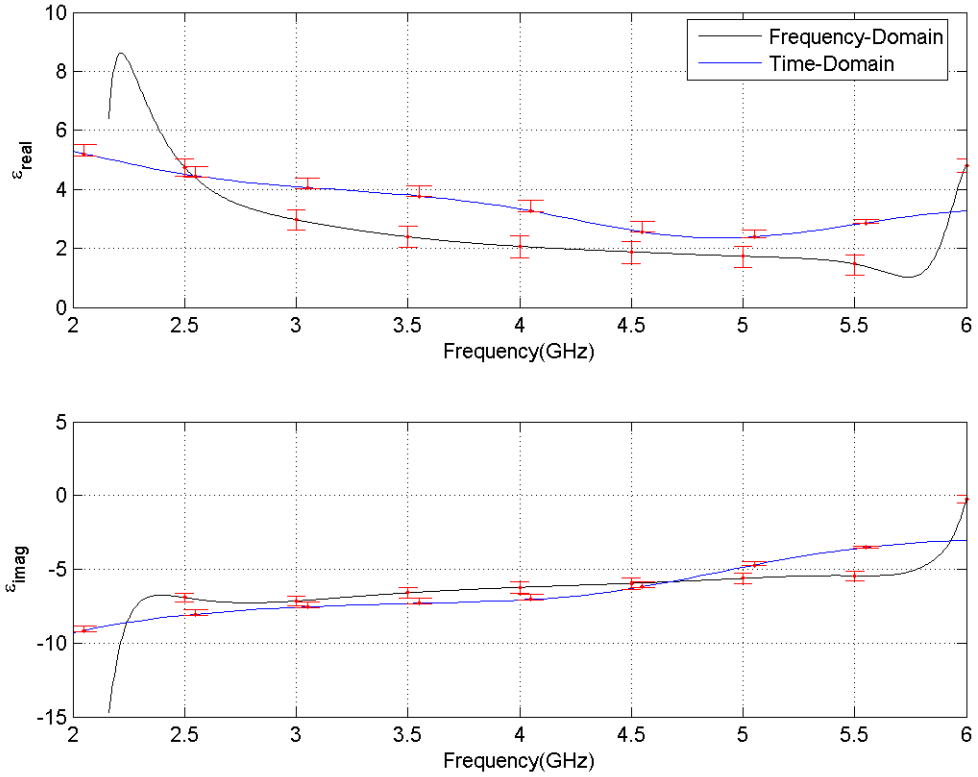

Figure A.5: Complex permittivity of 125 mil ERAM sample measured with the focus arch free-space system from 2-6 GHz for the frequency-domain method and direct time-domain method.

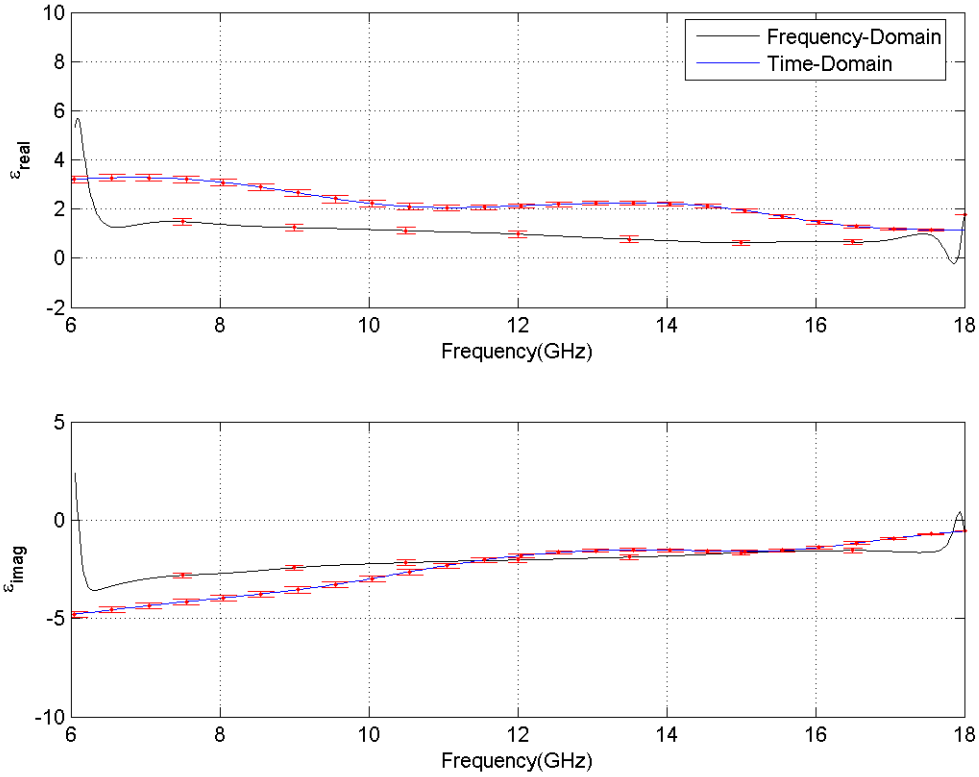

Figure A.6: Complex permittivity of 125 mil ERAM sample measured with the focus arch free-space system from 6-18 GHz for the frequency-domain method and direct time-domain method.

Bibliography

1. Barry, W. "A broad-band, automated, stripline technique for the simultaneous measurement of complex permittivity and permeability". *IEEE Transactions on Microwave Theory Techniques*, 34:80–84, January 1986.

2. Chen, L. F., C. K. Ong, C. P. Neo, V. V. Varadan, and V. K. Varandan. *Microwave Electronics Measurement and Materials Characterisation*. John Wiley & Sons, Inc., West Sussex England, first edition, 2004.

3. Collin, R. E. *Signal Processing And Linear Systems*. IEEE Press, New York, second edition, 1991.

4. Dorey, Sean P. *Stepped Waveguide Electromagnetic Material Characterization Technique*. Master's thesis, Graduate School of Engineering, Air Force Institute of Technology (AETC), Wright-Patterson AFB OH, March 2004. AFIT/GE0/ENG/04-01.

5. Edward J. Rothwell, Bradley Perry. *Time Domain Electromagnetic Field Reflectometry*. In-House AFRL-ML-WP-TR-2004, Michigan State University, East Lansing MI, December 2004.

6. Havrilla, Michael J. *Analytical and experimental techniques for electromagnetic characterization of materials*. Ph.D. dissertation, Michigan State University, East Lansing MI, 2001.

7. Hyde, Milo W. *Stepped Waveguide Electromagnetic Material Characterization Technique*. Master's thesis, Graduate School of Engineering, Air Force Institute of Technology (AETC), Wright-Patterson AFB OH, March 2006. AFIT/GE/ENG/06-24.

8. J. Baker-Jarvis, E. J. Vanzura and W. A. Kissick. "Improved technique for determining complex permittivity with the transmission/reflection method". *IEEE Transactions on Microwave Theory Techniques*, 38:1096–1103, August 1990.

9. Lathi, B. P. *Signal Processing And Linear Systems*. Berkeley-Cambridge Press, Carmichael CA, first edition, 1998.

10. Nicolson, A. M. and G. F. Ross. "Measurement of the intrinsic properties of materials by time-domain techniques". *IEEE Transactions on Instrumentation and Measurements*, 377–382, November 1970.

11. Wier, W. B. "Automatic measurement of complex dielectric constant and permeability at microwave frequencies". *Proceedings IEEE*, Vol.62. IEEE, 33-36, January 1974.

REPORT DOCUMENTATION PAGE

Form Approved
OMB No. 074-0188

PLEASE DO NOT RETURN YOUR FORM TO THE ABOVE ADDRESS.

1. REPORT DATE *(DD-MM-YYYY)*	**2. REPORT TYPE**	**3. DATES COVERED** *(From – To)*
23–03–2006	**Master's Thesis**	Sept 2004 — Mar 2006

4. TITLE AND SUBTITLE

Investigation of Frequency-Domain and Time-Domain Free-Space Material Measurements

5a. CONTRACT NUMBER

5b. GRANT NUMBER

5c. PROGRAM ELEMENT NUMBER

6. AUTHOR(S)

Kirt J. Cassell, Capt, USAF

5d. PROJECT NUMBER
If funded, enter ENR #

5e. TASK NUMBER

5f. WORK UNIT NUMBER

7. PERFORMING ORGANIZATION NAMES(S) AND ADDRESS(S)

Air Force Institute of Technology
Graduate School of Engineering and Management (AFIT/EN)
2950 Hobson Way
WPAFB OH 45433-7765

8. PERFORMING ORGANIZATION REPORT NUMBER

AFIT/GE/ENG/06-12

9. SPONSORING/MONITORING AGENCY NAME(S) AND ADDRESS(ES)

Dr. George R. Simpson
AFMC/AFRL/SNS
2951 K Street
WPAFB, OH 45433 DSN: 785-0279 george.simpson@wpafb.af.mil

10. SPONSOR/MONITOR'S ACRONYM(S)

11. SPONSOR/MONITOR'S REPORT NUMBER(S)

12. DISTRIBUTION/AVAILABILITY STATEMENT

APPROVED FOR PUBLIC RELEASE; DISTRIBUTION UNLIMITED

13. SUPPLEMENTARY NOTES

14. ABSTRACT

Electromagnetic material characterization is the process of determining the complex permittivity and permeability of a test sample. The primary goal of this thesis is to develop a new two transmission material measurement method to decrease the error associated with using a reflection measurement. The transmission method uses a sample transmission measurement and a acrylic backed sample transmission measurement. This technique is first demonstrated in a rectangular waveguide system then extended to frequency-domain and time-domain focus arch free-space systems. The frequency-domain free-space calibration process decreases accuracy at the band edges. The use of a digital oscilloscope with a time-domain reflectometer (TDR) module should increase accuracy by removing the windowing and transforming operations and is a secondary goal of this thesis. Experimental results of the ϱ_r and μ_r values of a magnetic radar absorbing material (MRAM) sample for the three measuring devices are presented. The two transmission method is compared to the NRW method to validate the two transmission method in all three measuring devices.

15. SUBJECT TERMS

material measurement, magnetic materials, permittivity(electrical), permeability(magnetic), transmission(waves), time-domain, free-space

16. SECURITY CLASSIFICATION OF:			**17. LIMITATION OF ABSTRACT**	**18. NUMBER OF PAGES**	**19a. NAME OF RESPONSIBLE PERSON**
REPORT	**ABSTRACT**	**c. THIS PAGE**			Michael J. Havrilla (ENG)
U	**U**	**U**	**UU**		**19b. TELEPHONE NUMBER** *(Include area code)* (937) 255–3636, ext 7252

Standard Form 298 (Rev: 8-98)
Prescribed by ANSI Std. Z39-18